THESIS FOR THE DEGREE OF LICENTIATE OF ENGINEERING

Catalytic Upgrading of Waste Oils to Advanced Biofuels – Deactivation and Kinetic Modelling Study

Prakhar Arora

CHALMERS
UNIVERSITY OF TECHNOLOGY

Chemical Engineering Division
Department of Chemistry and Chemical Engineering
CHALMERS UNIVERSITY OF TECHNOLOGY
Gothenburg, Sweden 2018

Catalytic Upgrading of Waste Oils to Advanced Biofuels – Deactivation and Kinetic Modelling Study

Prakhar Arora

© Prakhar Arora, 2018.

Licentiatuppsatser vid Institutionen för kemi och kemiteknik
Chalmers tekniska högskola.
Nr 2018:11

Department of Chemistry and Chemical Engineering
Chalmers University of Technology
SE-412 96 Gothenburg
Sweden
Telephone + 46 (0)31-772 1000

Cover:
Graphical illustration of conversion of different waste oils to green diesel (HVO) during catalytic hydrodeoxygenation process.

Printed by Chalmers Reproservice
Gothenburg, Sweden 2018

Catalytic Upgrading of Waste Oils to Advanced Biofuels – Deactivation and Kinetic Modelling Study

Prakhar Arora

Department of Chemistry and Chemical Engineering
Chalmers University of Technology, Gothenburg 2018

Abstract

The demand for liquid hydrocarbons as transportation fuels is enormous and ever growing. Advanced biofuels is one of the promising solutions to keep pace with the global transition to cleaner energy by reducing greenhouse gas emissions from the transport sector. It is possible to selectively remove oxygen from waste oils like tall oil, used cooking oil etc. via a catalytic hydrodeoxygenation (HDO) process to produce advanced biofuels. These biofuels have similar molecules as in the traditional fossil-based fuels and exhibit improved performance. This thesis focuses on aspects of catalyst deactivation and kinetic modelling of HDO reactions.

In the first study, the influence of iron (Fe) as a poison during HDO of a model compound for renewable feeds (Oleic acid) over molybdenum based sulfided catalysts was investigated. Fe is a potential contaminant in renewable feeds due to corrosion during transportation and storage in iron vessels. A series of experiments with varying Fe-oleate concentration in the feed over MoS_2/Al_2O_3 and $NiMoS/Al_2O_3$ catalysts. There was a salient drop in the activity of the catalysts. At higher Fe concentration, for the NiMoS catalyst, the selectivity for the direct hydrodeoxygenation product (C18 hydrocarbons) increased. However, it was opposite for the MoS_2 catalyst. There was a decrease in the yield of direct hydrodeoxygenation products and an increase in yield of decarbonated products. It was proposed that Fe interacted with these two catalyst systems differently. Fe influenced the critical step of creation of sulfur vacancies in a negative way which resulted in lower activity. Microscopic analysis indicated that Fe was preferentially deposited close or around the nickel promoted phase, which explained why the role of Ni as a promoter for the decarbonation route was subdued for the NiMoS catalyst.

In the second study, the kinetics during HDO of stearic acid (SA) over a sulfided $NiMo/Al_2O_3$ catalyst were explored to investigate the reaction scheme. Model compounds like octadecanal (C18=O) and octadecanol (C18-OH) were employed to understand the reaction steps and quantify the selectivity. A Langmuir–Hinshelwood-type kinetic model was used to investigate the kinetics. The results from the proposed kinetic model were found to be in good agreement with experimental results. In addition, the model could effectively reproduce the observed experimental profiles of different intermediates like C18=O and C18-OH and illustrate phenomena like inhibiting effects of the fatty acid.

Keywords: Advanced biofuels, Hydrodeoxygenation, Catalytic HDO, NiMo, MoS_2, TEM, Stearic acid, Oleic acid, Kinetic modelling

"The meeting of two personalities is like the contact of two chemical substances: if there is any reaction, both are transformed"

Carl Jung

Acknowledgements

I would like to acknowledge the many people who supported me and contributed to this thesis. I am deeply grateful and want to express my sincere gratitude to the following people-

First of all, I acknowledge my main supervisor Prof. Derek Creaser for his ardent supervision and perpetual encouragement. Thanks for channeling my curiosity into the shaping of this research project. I have thoroughly cherished our many scientific discussions and am looking forward for future ones.

My co-supervisor, Prof. Louise Olsson, who has been very supportive in my research. Many thanks for our fruitful discussions and the feedback. I appreciate your advice a lot.

Prof. Magnus Skoglundh, the director of KCK and all senior members for creating an atmosphere of scientific curiosity in KCK.

I am thankful for this exciting project given by our industry partner Preem AB. Many thanks to Eva Lind Grennfelt and Stefan Nyström for sharing their refinery experience and engaging discussions.

My officemate, Houman, thanks for all help and the interesting conversations we had. Salam, thanks for your help in the lab and my experiments. I really appreciate your scientific inputs in my research. Colleagues who helped me with research, teaching and friends at after work and parties with whom I have had deep conversations about life and what not- Lidija, Nadya, Xavier, Ida, Aiyong, Patric, Rasmus and Mattias. Thanks to previous colleagues who helped in research/teaching- Stefanie, Oana, Kurnia, Muzamal and Kunpeng. I would also like to acknowledge all colleagues at KCK and KRT. It was a pleasure to work, discuss and grow with you.

Friends and colleagues outside this department – Stefan, Behabitu, Nico, Khushbu, Sandeep, Sangamesh, Tushar, Arun, and Sandra.

I would like to mention a few names who have influenced me in different ways and played a role of mentor at different point of time in my life – Dr. S.R. Sharma, Dr. Neelesh Dahanukar, Dr. V.G. Anand, Dr. Dharmesh Kumar, Dr. Martin Linck and Anders Hultgren.

Malin and Eva, thanks for your support.

Also my old friends who have been with me for a long time- Subhajit, Ashutosh, Nishtha and Dhanraj.

Marco and Katarina for your excellent contributions during your master thesis projects. I benefited a lot as a co-supervisor of your master's project and I am glad to see you doing well in your careers.

My girlfriend and partner for every adventure of life, Michelle. Thanks for being a proofreader for this thesis.

π for always giving a warm hello when I arrive home after a day´s work. Your playfulness and mischievous activities brighten my days.

My parents, Pratibha and Sunil, who have always supported me and blessed me with unconditional love. My brother and his wife, Dr. Shashank and Dr. Rashi, who have always encouraged me to pursue my dreams. My adorable niece, Ladoo (Aadita) whose pictures and videos have cheered me up even from such a distance.

This work is performed at the Competence Centre for Catalysis in collaboration with Preem. We would like to acknowledge Formas (Contract: 239-2014-164) and Preem for the financial support. The Competence Centre for Catalysis is hosted by Chalmers University of Technology and financially supported by the Swedish Energy Agency and the member companies AB Volvo, ECAPS AB, Haldor Topsøe A/S, Scania CV AB, Volvo Car Corporation AB, and Wärtsilä Finland Oy.

List of publications

I. Investigating the effect of Fe as a poison for catalytic HDO over sulfided NiMo alumina catalysts
Prakhar Arora, Houman Ojagh, Jungwon Woo, Eva Lind Grennfelt, Louise Olsson, Derek Creaser
Applied Catalysis B: Environmental, Volume 227, 2018, Pages 240-251 (https://doi.org/10.1016/j.apcatb.2018.01.027)

Contribution: I planned and defined the scope with co-authors. I performed the experiments in this study. I interpreted the results with co-authors, and wrote the first draft of manuscript.

II. Kinetic study of hydrodeoxygenation of stearic acid as model compound for renewable oils
Prakhar Arora, Eva Lind Grennfelt, Louise Olsson, Derek Creaser (*in Manuscript*)

Contribution: I planned and defined the scope with co-authors. I performed the experiments in this study. I was assisted by Derek Creaser with simulations. I interpreted the results with co-authors, and wrote the first draft of manuscript.

Publications not included in this thesis

I. Effect of Dimethyl Disulfide on Activity of NiMo Based Catalysts Used in Hydrodeoxygenation of Oleic Acid
Houman Ojagh, Derek Creaser, Stefanie Tamm, Prakhar Arora, Stefan Nyström, Eva Lind Grennfelt, and Louise Olsson
Industrial & Engineering Chemistry Research 2017 56 (19), 5547-5557 (http://dx.doi.org/10.1021/acs.iecr.6b04703)

List of abbreviations

BET	Brunauer Emmett Teller
BJH	Barret Joyner Halenda
BSTFA	N,O-Bis(trimethylsilyl)trifluoroacetamide
C17+	Saturated and unsaturated isomers of C17 hydrocarbons
C18+	Saturated and unsaturated isomers of C18 hydrocarbons
C18=O	Octadecanal
C18-OH	Octadecanol
CUS	Coordinately unsaturated sites
DCO	Decarbonylation
DCO_2	Decarboxylation
DCO_x	Decarbonation
DMDS	Dimethyl disulfide
DSC	Differential scanning calorimeter
EDX	Energy dispersive x-ray
EOS	Equation of state
FAs	Fatty acids
FFA	Free fatty acid
FID	Flame ionization detector
GC	Gas chromatography
GDP	Gross domestic product
GHG	Greenhouse gas
HAADF	High angle annular dark field
HDO	Hydrodeoxygenation
HDM	Hydrodemetallization
HDN	Hydrodenitrogenation
HDS	Hydrodesulphurisation
HEFA	Hydroprocessed Esters and Fatty Acids
HR-TEM	High resolution transmission electron microscopy
HVO	Hydrotreated Vegetable Oil

ICP-SFMS	Inductively coupled plasma sector field mass spectrometry
LGO	Light gas oil
MS	Mass spectrometer
MTOE	Million tonnes of oil equivalent
OA	Oleic acid
OPEC	Organization of the petroleum exporting countries
PAHs	Polynuclear aromatic hydrocarbons
PSRK	Predictive Soave-Redlich-Kwong
RPM	Revolutions per minute
SA	Stearic acid
SEM	Scanning electron microscopy
SSR	Squares of the residuals
STEM	Scanning transmission electron microscopy
TAN	Total acid number
TCD	Thermal conductivity detector
TEM	Transmission electron microscopy
TGs	Triglycerides
TMS	Transition metal sulfides
TOFA	Tall oil fatty acid
TPR	Temperature programmed reduction
VGO	Vacuum gas oil
VLE	Vapor liquid equilibrium
XPS	X-ray photoelectron spectroscopy

Contents

1 Introduction

1.1 World's Energy Trends and Challenges

The world's need for energy is ever-growing with widespread socio-economic development and a rising population. There is a spatio-temporal shift in the global energy landscape, whether it is about the movement of consumption centers to countries like China and India or the evolving global energy mix from coal to wind and solar due to technological advancements. Rapid growth in population and improving prosperity, with the GDP expected to double in the next two decades, will result in energy consumption going from 13,276 Mtoe (million tonnes of oil equivalent) in 2016 to 17,983 Mtoe in 2040 [1]. At present, coal stands for the lion share, i.e. over 63% out of all fossil fuels (incl. coal, petroleum and natural gas), for the production of electricity. With technological innovations and falling costs, solar and wind could drive the increased electrification of the future. Wind and solar are expected to contribute to 48% of installed capacity and 34% of electricity generation world-wide by 2040 [2]. This is a leapfrog growth compared with just 12% and 5% today.

Renewables (including hydropower) are the fastest-growing sources for generation of electricity over the next 25 years, rising by an average of 2.8% per year, as technological improvements and government incentives in many countries support their increased use [3]. Coal is already on decline in several countries, while it is still expected to peak in China. With many recent major discoveries of gas and shale gas, they could act as transition fuels for power generation by quickly replacing coal. Gas-fired power plants are quick to start compared to giant coal plants. These gas-to-electricity plants could provide system stability to a fraction of the baseload. With the improvement in technology of photovoltaic cells and turbines they are becoming more energy efficient and declining in cost every year [4]. Even though power generation from solar and wind is intermittent, still with sufficient capacity they could account for the remaining baseload and a majority of the intermediate load. Power requirement at peak load times could be supplied by giga-battery packs which could be charged from solar or wind when the demand is low. With the integration of technologies like blockchain based smart grids and demand-side response (DSR), this mix of renewable sources could eliminate our dependence on coal for electricity production [5, 6].

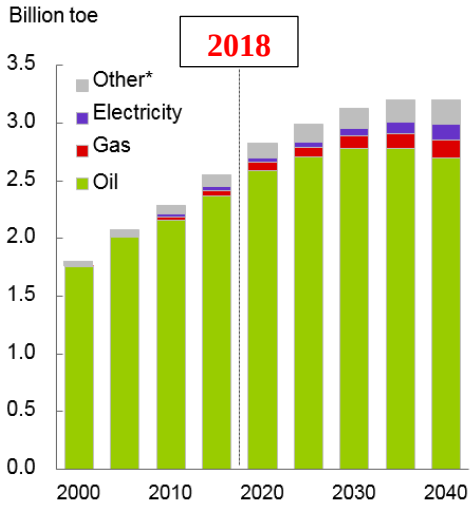

Fig 1: Transport energy consumption by fuel type. *Other includes biofuels like HEFA, XTL condensates, hydrogen [1].

While solar and wind potentially herald the solutions to replace coal for electricity production and a transition towards energy sources with lower emissions is made, the picture to replace petroleum is more challenging. Advancements in ways of mobility have shrunk our world, while opening up new panoramas and possibilities. Fig 1 represent the energy demand from the transport sector. Worldwide, petroleum and other liquid fuels are the dominant sources of transportation energy, although their share of total transportation energy is expected to decline from 94% as of today to 85% in 2040 [1]. The transport sector could be divided into five segments – light duty (cars and two-wheelers), heavy duty (trucks, SUVs etc.), marine (ships etc.), aviation and rail. Continuing urbanization and a significant expansion of the middle class in many parts of the world will increase the cars on the roads and total miles travelled per year. Though with the evident arrival of electric vehicles (EVs) and plug-in hybrid electric vehicles (PHEVs) there will be some slowdown in demand for petroleum products, especially from the light duty vehicle segment in the future. However, the availability of a charging infrastructure and scarcity of lithium for battery production could limit the penetration of electric vehicles to the masses. Ballooning GDP per capita all across the world drives the trade and commercial activities which are supported by heavy vehicles (trucks), ship and rail. Although electrification of railways has taken a quantum jump in the last few years, it would be a long while before electricity will be powering the trucks on roads and ships on water in a viable way. Also, people are increasingly traveling to explore and for business purposes. Unfortunately it is not possible to use batteries to fly planes and we are dependent on liquid hydrocarbon fuels for air travel. To give some perspective, global per capita CO_2 emissions are at five metric tons while a commercial round trip flight from Europe to New York emits about one metric ton of CO_2 per person [7]. This trivial fact reminds us of the gravity of the situation and the impact of aviation on the environment. So there is a dire need to invest our efforts in developing alternative technologies and renewable fuels for the transportation sector.

A rise in personal mobility, increasing trade of goods and services and growth in leisure travel are all endorsing the higher energy demand in the transportation sector. So there seems to be no brake to the growing demand for petroleum products for the transportation sector. However, there is hope as many countries are pledging to reduce their dependence on fossil fuels. In Sweden, the government has an ambitious target to reduce the emissions from transport sector

by 70% by 2030. This would enable Sweden to progress toward their goal to have no net emissions of greenhouse gases into the atmosphere by 2045 [8]. There are a few intangible factors like an increase in efficiency of engines, a rise in awareness among the population to use public transport or car-pooling and the inevitable arrival of autonomous vehicles on our roads that contribute to a fossil-free transport sector. These factors are each incremental in nature and would occur over varying timelines but, nonetheless, any steps to combat climate change are commendable. Also, it is envisioned that there will be no silver bullet to mitigate climate change. Instead there will be thousands of such solutions towards a greener economy.

1.2 Contribution of bio-resources to world energy needs

Biomass and its related resources present a plausible solution to bridge the world's widening energy gap. Bio-resources include agriculture residues like bagasse and rice husk etc., forest residues like tree stumps, industrial wastes like tall oil and other waste bio-oils like waste cooking oils, non-edible vegetable oils, fats and greases etc. All these renewable bio-based feedstocks do not compete with food or land usage and are almost carbon neutral. Another advantage with these bio-based feedstocks are that they are uniformly distributed in the world unlike petroleum resources. According to a recent geological survey, more than 80% of the world's proven crude oil reserves are located in countries who are members of OPEC, with the majority (around 65%) of OPEC oil reserves situated in the Middle East [9].

These bio-based feedstocks could be converted to energy using distinct pathways like enzymatic and thermochemical conversion. The enzymatic method is highly selective, but high costs and issues related to scale-up are major hurdles blocking their commercial use. Thermochemical conversions, including pyrolysis, gasification, and combustion etc. are a few ways to convert bio-based feedstocks to energy. As nature takes millions of years to convert fossils to coal, petroleum and gas, the same could be achieved in just a few seconds at high temperature during thermochemical conversion of biomass. The process of thermochemical conversion could be configured in different ways to transform biomass to yield heat, electricity, or gaseous or liquid precursors for upgrading to liquid fuels or chemical feedstocks or even drop-in fuels!

Direct combustion is still a dominant pathway but it has very poor energy recovery. Pyrolysis of biomass is thermal decomposition in the absence of oxygen to produce pyrolysis oil as a liquid product. It could be classified as flash, fast or slow pyrolysis depending on the residence time. Two major limitations in this pathway is that pyrolysis oil contains a high oxygen content and is not stable. So it has to be upgraded to remove oxygen for fuels or chemicals. However, there are a few promising technologies like IH^2, in which vapors produced during hydropyrolysis are catalytically upgraded before condensation [10]. Biomass gasification is another such route in which the exothermic partial oxidation of biomass yields a mixture of gases rich in CO, H_2, CH_4 and CO_2. Then the gas stream could undergo a processing step after which either it could be directly used as fuel or upgraded to paraffin waxes or chemical feedstocks. Apart from the additional cost from the processing and pressurizing step, the tars from higher molecular weight volatiles poses a major challenge during biomass gasification. The management of tars, which are basically polynuclear aromatic hydrocarbons (PAHs), during biomass gasification is a challenge since they are environmental pollutants and can impact stable operations of the plant [11].

HEFA (Hydroprocessed Esters and Fatty Acids), also known as HVO (Hydrotreated Vegetable Oil), is a renewable diesel fuel that can be produced from a gamut of feedstocks like animal fats and

grease, waste vegetable oils, and forestry residues like tall oil. These various renewable feedstocks could be hydroprocessed stand alone or co-fed with petroleum feedstock as well [12].

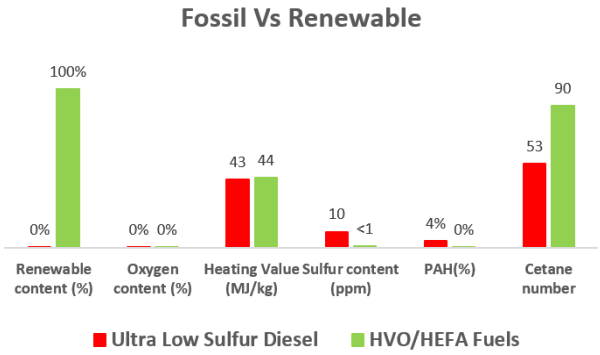

	Ultra Low Sulfur Diesel	HVO/HEFA Fuels
Renewable content (%)	0	100
Oxygen content (%)	0	0
Heating Value (MJ/kg)	43	44
Sulfur content (ppm)	10	1
Polyaromatics (%)	4	0
Cetane number	53	90
GHG emissions	Baseline	-90%
PM emissions	Baseline	-46%
Nox Emissions	Baseline	-14%
Storage stability	Baseline	Good

Fig 2: Comparison of HVO/HEFA and a conventional low-sulfur diesel fuel [13].

When such renewable fuels are used then atmospheric carbon is recycled, while in the case of fossil fuels prehistoric carbon stored in the earth's crust is introduced into atmosphere when they are burnt. HEFA fuels are chemically identical to the fossil based hydrocarbons. They could be blended with the "bottoms" of diesel pools as they have much higher cetane numbers. They are advantageous as they employ the existing infrastructure for refining, transportation via pipelines, storage tanks and the existing automotive fleet with no need for engine modification. In fact, HEFA fuels are premium fuels because of their higher heating value, lower SOx and NOx emissions, and reduced levels of polyaromatic hydrocarbons (PAH) and fine particulates [13]. Fig 2 illustrates some of the advantages of HEFA fuels over tradition diesel fuel. Additionally, these HEFA fuels have lower greenhouse gas (GHG, gCO_2 eq/MJ) emissions by up to 90% over the lifecycle of the fuel compared to fossil based diesel [14]. Currently, annual capacity for HEFA fuels is over 2.6 billion litres, and growing at a steady rate [15]. There are several refineries from Neste, ENI, Total, Preem and Repsol producing these renewable HEFA fuels. NEXBTL™, Ecofining™, Vegan™ & Hydroflex are some of the commercial technologies employed in these refineries [16]. Several more refineries in France, Italy and Singapore are in the pipeline which would further boost the production of these advanced biofuels. It should be highlighted that the core of these refineries is the catalytic hydrodeoxygenation (HDO) process, which is the removal of oxygen from renewable feeds of bio-origin over a catalyst in the presence of hydrogen to produce predominantly water as a side product. Catalytic HDO will be discussed in detail in Section 2.1 of this thesis.

With all these benefits, HEFA fuels have a great potential to substantially decarbonize the world's economy. The demand for transport distillate – jet fuel, road and marine diesel – is growing. This rising demand could be supplemented by HEFA or HVO renewable fuels. Also the refining processes for these fuels could be tuned to produce hydrocarbons in gasoline, jet kerosene and the diesel range. This could inherently reduce our dependence on fossil fuels in the near future. Sometimes it is debated that electrification of the transport sector could solve all the climate change related problems. But what if the much-hyped future techno-economic visions for batteries for EVs do not come about at the foreseen pace, or are found to be unacceptable or too expensive for the driving public? It is not biofuels or electrification – both are essential to achieve a 30-40% decarbonization of the transportation sector. Thus there is a dire need to invest in resources from a research, awareness, production and policy-making point of view. In a recent report by IEA – Tracking clean energy progress 2017; transport biofuels was identified as an area

where more efforts are needed to be on track. The “2°C Scenario (2DS)” presents an outlook with at least a 50% chance of limiting the average global temperature increase to 2°C based on energy system deployment around the world and an emissions trajectory. This 2DS would also limit CO_2 emissions between 2015 and 2100 to 1 000 Gt CO_2 from the energy sector. The 2DS directs governments around the world to reduce CO_2 emissions by almost 60% by 2050 in comparison to 2013. It is projected that after 2050, carbon emissions would decline until carbon neutrality is reached.

1.3 Objectives and scope

The objective of this thesis is to investigate critical aspects of catalytic hydrodeoxygenation of fatty acids (FAs). FAs are a major component of several renewable feedstocks like tall oil, used vegetable oil etc. Since, renewable feedstocks have a high oxygen content and are corrosive in nature (high TAN), during transport and storage they react with iron vessels to form iron complexes. In the first study, we have elucidated the effect of iron (Fe) causing poisoning of NiMo and Mo catalyst during HDO. Activity measurements and spent catalyst characterization led to intriguing insights regarding the catalyst deactivation. To further understand the underlying chemistry and reaction kinetics, we carried out a set of experiments varying different parameters and used this data to develop a kinetic model that could predict the product selectivity based on the operating conditions.

2 Background

2.1 Catalytic hydrodeoxygenation

Hydrotreating is a process employed in refineries around the world to remove the hetero-atoms from fossil based feedstocks like Naphtha, vacuum gas oil (VGO) etc. Catalytic hydrotreating ranks as one of the most important petroleum refining processes along with cracking and reforming. Hydrotreating includes hydrodesulphurization (HDS), hydrodenitrogenation (HDN), hydrodeoxygenation (HDO) and hydrodemetallization (HDM) reactions to remove different impurities. Typically, in fossil feedstocks the oxygen content is not high, so not much attention has been paid to HDO. But renewable feedstocks like lignocellulosic biomass, pyrolysis oil, waste cooking oil, tall oil etc. can contain oxygen in a range of 10-40 wt%. Thus, HDO has been gaining a lot of attention lately as the challenges are different than the traditional HDS and HDN processes. HDO is a hydrotreating process in which oxygen is removed from the feeds in the presence of hydrogen at high temperature and pressure over catalysts [17]. Hydrogen is removed to produce side products like H_2O, CO and CO_2. There are several scientific and engineering problems associated with HDO processes which requires research efforts. To list a few:

a. A lot of water is produced as a side product which can be detrimental to the catalyst support and may contribute to excessive coking.
b. At the introduction of feed in a commercial scale reactor, since HDO is an exothermic process, the sudden rise in temperature could have devastating results which poses technological challenge for the design of the reactors.
c. Contaminants in renewable feeds are very different. It varies from metals like Na, Mg and Fe, to non-metals (Cl) and organic compounds (phospholipids) [16, 18, 19]. There is a sincere need to investigate their effect on the catalyst activity under different reaction conditions.

In this thesis, the focus would be on the hydrodeoxygenation of FAs and similar compounds like triglycerides (TGs) and methyl esters. TGs are the esters of glycerol with FAs while methyl esters are formed from the esterification of methanol with FAs. FAs have a carboxyl group (–COOH), with a long carbon chain of 14-24 carbons with 18-carbon FAs are most common [20]. Lauric, capric, palmitic, myristic, oleic, and stearic acids are some common FAs. Fig 3 shows a few model compounds from fatty acids, triglycerides and methyl ester classes of compounds. TGs and FAs form the major components of renewable feedstocks like oil from Jatropha, microalgal oil and tall oil [21-23]. Also waste cooking oil contains a high amount of free fatty acids (FFAs) which is

available in large amounts and can be used as a renewable feedstock. Hydrodeoxygenation of such feeds rich in FAs and TGs yields hydrocarbons which are known as renewable or green diesel.

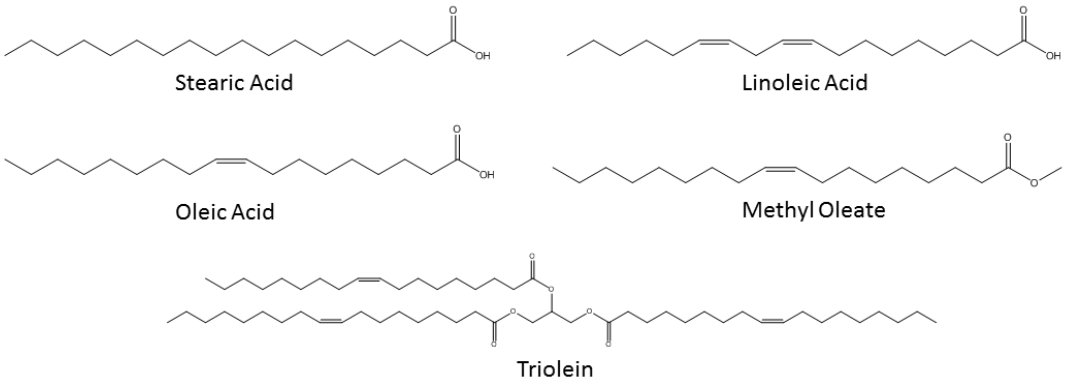

Fig 3: A few model compounds (fatty acids, methyl esters and triglycerides)

These various feedstocks can be processed with conventional hydrotreating catalysts like Ni or Co promoted molybdenum sulfide (MoS_2) supported on alumina in a refinery setup to produce hydrocarbons in a temperature range of 300-450 °C and hydrogen pressures of 50-180 bar. These processes have high yields and carbon recovery rates. The reaction chemistry for TGs, methyl esters and FAs is quite similar. Among the latter two, FAs are the most common intermediates. These reactions initiate with the hydrolysis of the ester group present in TGs or alkyl esters and saturation of double bonds in the long alkyl chain, if any. The hydrolysis reaction occurs on the Lewis acidic sites of the alumina support [24] while the active sites on the metal enables the hydrogenation reaction. Then FAs undergo deoxygenation which include hydrodeoxygenation, decarboxylation, decarbonylation. Other reactions include cracking and hydrogenation to produce hydrocarbon final products mostly as straight chain alkanes. Meanwhile the carbon backbone of TGs is converted into propane and other gaseous products including CO, CO_2, H_2O and CH_4 are produced. We will limit our discussions to FAs only in this study.

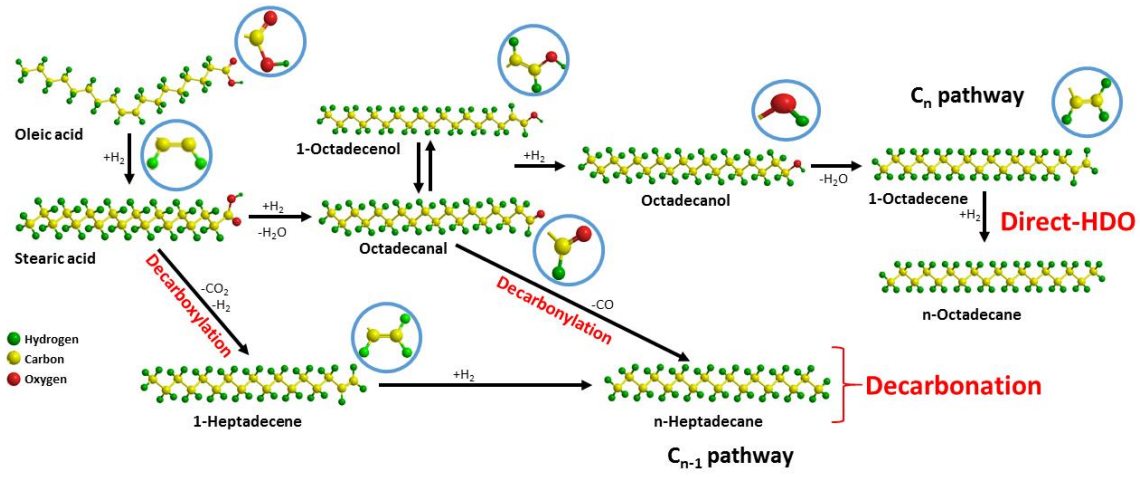

Fig 4: Reaction scheme for hydrodeoxygenation of oleic acid (OA)

Fig 4 describes the reaction scheme of hydrodeoxygenation of OA. Deoxygenation of FAs over transition metal sulfides (TMS) catalysts happens in following three ways-

a) A so called direct-HDO in which oxygen is removed as a water (H_2O) molecule

b) Decarbonylation (DCO) in which oxygen is removed as carbon monoxide (CO)

c) Decarboxylation (DCO_2) in which oxygen is removed as carbon dioxide (CO_2)

In the first route, a C_n alkane or alkene is formed as the final product with same number of carbon as in the fatty acid. In the latter two routes, a hydrocarbon (alkane or alkene) is formed with one less carbon.

For this thesis, the term decarbonation (DCOx) will be used to refer collectively to decarbonylation and decarboxylation, otherwise they will be separately stipulated. It should be noted that the hydrodeoxygenation or "HDO" is a broader term to define removal of oxygen while "direct-HDO" is specifically used when oxygenated products are converted to produce water as the side product.

2.2 Transition metal sulfides for HDO of FA

In a refinery complex, production of liquid transportation fuels contribute to a major share in the revenues generated. Crude oil could be broadly classified based on its sulfur content; less than 0.7% sulfur content is called Sweet and greater than 0.7% sulfur content is called Sour. Crude oil is distilled into lighter fractions to produce a mix of liquid fuels like gasoline, jet kerosene and diesel. In between they have to be further upgraded to meet the fuel specifications of the respective country. For example as of now the maximum limit of sulfur is 10 ppm in Europe, 15 ppm in USA and 10 ppm for on-road diesel while 50 ppm for off-road diesel in China. Meanwhile the fractions coming from the distillation tower, like light gas oil (LGO) or vacuum gas oil (VGO) from the vacuum unit have a relatively high sulfur content. So transition metal sulfides (TMS) have been traditionally employed in the refineries for hydrotreating processes. They are quite effective in removal of heteroatoms like sulfur and nitrogen, oxygen, halides and metals like V etc. However, in the petroleum industry TMS catalysts are used mainly for hydrodesulfurization (HDS) and hydrodenitrogenation (HDN). A typical composition of a TMS catalyst is cobalt or nickel promoted molybdenum-tungsten on a porous support such as alumina. They are in oxidized form when synthesized and then need to be sulfided in the presence of a sulfiding agent to form the active sulfided phase. These TMS catalysts have been found potent even for HDO reactions due to the similarity between the sulfur and oxygen atom.

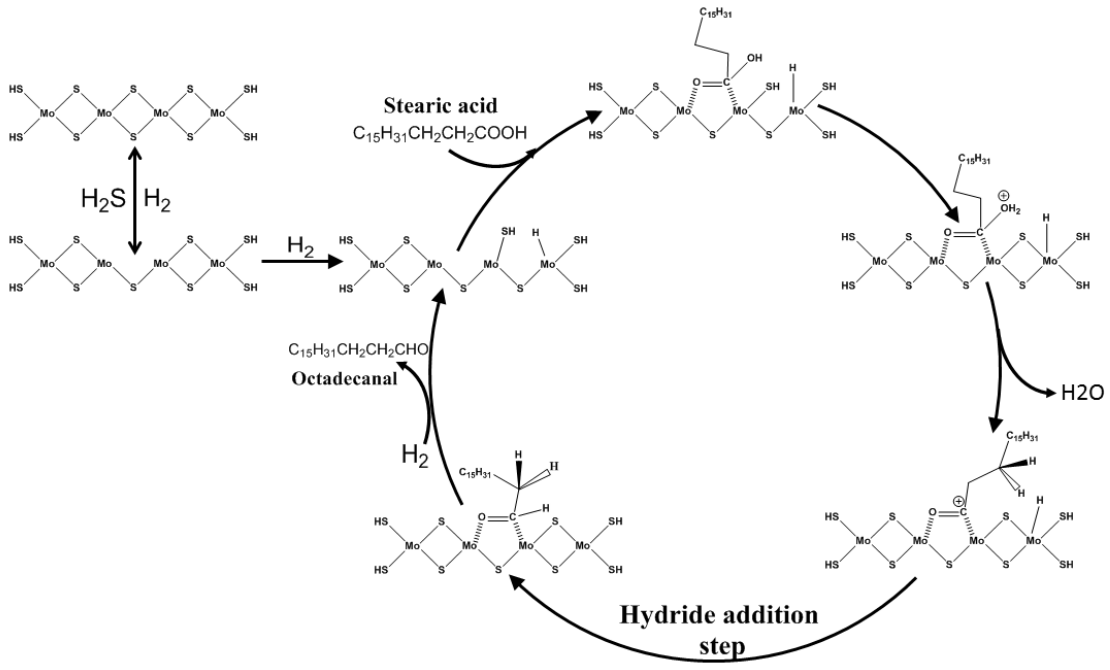

Fig 5: Catalytic cycle for first step of conversion of stearic acid (SA) to octadecanal (C18=O) in the overall reaction scheme

Fig 5 depicts a proposed catalytic cycle for HDO of a FA molecule on TMS [25]. The first step is the creation of sulfur vacancies as sulfur from MoS_2 reacts with hydrogen to produce H_2S. There is always a dynamic equilibrium of these sulfur vacancies depending on H_2/H_2S ratio of the gas phase. Mortensen et al have suggested a similar catalytic cycle for a phenolic molecule that also starts with the creation of a sulfur vacancy [26]. Then a heterolytic dissociation of hydrogen molecule occurs which leads to a metal hydride (Mo-H) and sulfhydryl (-SH) group. A fatty acid molecule is adsorbed on the sulfur vacancy via its carbonyl group. This step is also consistent with that suggested by a DFT study [27]. After adsorption, the protonation of the hydroxyl group of the fatty acid molecule occurs by the SH group which is acidic in nature. In the next step, a water molecule is removed in tandem with the transfer of charge to carbon. This cation species undergoes a hydride addition step to yield the corresponding aldehyde. Finally, a hydrogen molecule reacts to yield a species with metal hydride (Mo-H) and sulfhydryl (-SH) which completes the catalytic cycle for conversion of stearic acid to octadecanal. NiMo (CoMo) catalysts were the first to be employed for the deoxygenation of molecules containing a carboxyl group like TGs, esters and FAs. Craig et al employed the sulfided form of transition based commercial catalysts for hydroprocessing of different vegetable oils like canola oil, palm oil, and soybean oil and renewable feedstocks like tall oil [28]. It yielded liquid paraffinic hydrocarbons in the C_{15} -C_{18} range with high cetane values. Laurent and Delmon tested hydrodeoxygenation of model compounds containing ester groups over CoMo/y-Al_2O_3 and NiMo/y-Al_20_3 catalysts [29]. They made an intriguing observation that the selectivity for the decarboxylation route decreases with the conversion of acids as there might be a competitive adsorption between the carboxylated reactants and hydrogen on the active sites. A comparative study over sulfided Ni, Mo and NiMo catalysts determined that Ni and Mo catalysts produce almost exclusively C_{17} and C_{18} hydrocarbons, respectively, while NiMo yields both hydrocarbons. Also it was concluded that the Ni/(Ni+Mo) ratio (range 0.2 to 0.4) is not so critical for the activity and selectivity of these catalysts

during HDO of TGs [30]. It is known that for traditional TMS catalysts employed for the HDS reaction, a ratio of 0.3 is preferred [31]. In another study to understand the exclusive role of active metal species and to separate the influence of support, unsupported TMS catalysts were tested [32]. Unsupported CoMo and NiMo catalysts were synthesized by the hydrothermal method then used in deoxygenation of vegetable oils. Based on the temperature programmed reduction (TPR) and experimental results, it was proposed that the Ni promoted catalysts have a higher hydrogenation activity attributed to an improved ability to create sulfur vacancies at lower temperature while CoMoS catalysts facilitated C-C bond cleavage on the saturated sites. These unsupported catalysts offer insignificant external mass transfer resistance. There was a recent study which comprehensively looked at the HDO of a range of model compounds (methyl oleate, oleic acid, triolein) over NiMo sulfide catalysts. It looked into the effect of temperature and pressure on the activity and selectivity during HDO. Even though NiMo and CoMo catalysts are widely popular for the refinery scale production of biofuels, there is still extensive research ongoing on novel catalysts for upgrading of FAs etc.

2.3 Other catalyst systems for HDO of FA

It is often debated that sulfided catalysts are not the best candidates for the upgrading of renewable feedstocks containing oxygen. This is mainly due to the reasons that sulfur leaching from these catalyst systems would contaminate the final product since oils from bio-origins have a low innate sulfur content. Many of these “sulfur-fee” alternative catalyst systems involve noble metals. The high cost of noble metals could be a barrier for scale-up of these catalyst systems, but they have contributed to develop an understanding of reaction mechanisms. In one pioneering work, Murzin and coworkers screened a broad range of catalysts - Ni, Mo, Pd, Pt, Ir, Ru, Rh, and Os on Al_2O_3, Cr_2O_3, MgO, and SiO_2 and activated C for deoxygenation of SA in a batch reactor. They found that Pd/C was the most active catalyst and established the promoting effect for deoxygenation in the following order Pd>Pt>Ni>Rh>Ir>Ru>Os [33]. However, all these catalyst systems are essentially only exclusively active for the decarbonation route. A novel sulfur-free catalyst with Ni supported on zeolite HBeta was used for deoxygenation of microalgal oil rich in FAs [34]. It was reported that this catalyst had a high selectivity for the HDO route i.e. C_{18} products with less than 1% of cracking. In a very recent study, bimetallic Pd-Au catalysts was postulated to be more stable than Pd/SiO_2 which deactivates rapidly during deoxygenation of OA due to self-poisoning of reactant molecules [35].

2.4 Catalyst Deactivation during HDO of FA

TMS catalysts are quite versatile and are effective for the hydrogenolysis of the bond between carbon and heteroatoms (like S, N, O etc.). These reactions occur on the active sites of the catalysts. But with time and exposure to feed these catalysts eventually undergo some degree of deactivation. It could be due to different reasons including loss of active sites, blocking of pore mouths, sintering etc. Although with respect to deactivation of TMS during HDO of FA, it mostly occurs due to the following phenomenon:

a. Loss in sulfidity of the catalyst

b. Coking

c. Inhibition due to water

d. Poisons present in renewable feedstocks

As the TMS catalysts are most active only in in the sulfide phase, a sulfiding agent like H_2S or DMDS has to be co-fed to keep the catalysts sulfided. TMS catalysts based on MoS_2 have it as a monolayer or clusters of slabs distributed over an alumina surface. These hexagonally shaped slabs have coordinatively unsaturated sites (CUS) a.k.a sulfur vacancies [17, 31]. These vacancies are of a Lewis acid character and it is where O containing molecules (like FAs) are adsorbed and undergo heterolytic cleavage. The role of the promoters like Ni (or Co) is to decrease the interaction of MoS_2 with alumina which results in considerably more active sites when compared to unpromoted MoS_2. However, it is plausible that some reactant molecules (like carboxylates) or poisons (like alkalis in renewable feeds) bind strongly or even irreversibly to subdue the labile nature of these sulfur vacancies. Since the sulfur content of renewable feeds rich in FAs like waste cooking oil, tall oil etc. is very low, during their upgrading there is a continuous input of a source of sulfur. There are a few studies which have covered different aspects of the pertinence of keeping the catalysts in sulfided form. Activity of NiMo catalysts were found to be more sensitive compared to CoMo for maintenance of the sulfide phase during HDO of a carboxylic ester group [36]. It was also reported that hydrogen sulfide results in increased selectivity towards the decarboxylation route. To compare the effect of different sulfiding agents, Senol et al investigated HDO of aliphatic esters on NiMo and CoMo catalysts while varying the concentration of H_2S and CS_2 [37]. The promotion effect of H_2S on total conversion of esters was found to be linear to its concentration, as it resulted in increased catalyst acidity. However, CS_2 suppressed the acid-catalyzed reactions resulting in lower HDO conversions.

Catalyst coking occurs when adsorbed species polymerize or condense into complex larger units in the catalyst pores. This phenomenon could have a deteriorating impact on the pore volume of the catalyst. Coking is known to be ubiquitous and inevitable, but it is aggravated by feeds containing aromatics or heterocyclics, or in a hydrogen deficient environment or due to the presence of water. Immediate catalyst deactivation due to coking was observed during deoxygenation of unsaturated FAs over Pd/C at 300 °C under a scarce hydrogen (1 vol%) environment in dodecane as a solvent [38]. There was a related study to understand the nature of deactivation on supported Pd catalysts [39]. An extensive characterization was done using XPS and TEM to conclude that there was no oxidation of the Pd surface with no sintering of Pd particles. Physisorption and chemisorption results suggested that a large loss of surface area and pore volume which pointed to strong adsorption of organic species.

Catalyst activity could be inhibited due to presence of water as it can oxidize the active sulfide phase of these catalysts. There was a slight negative effect on the HDO activity at lower (<5000 ppm) concentrations of water, while at higher amounts the effect was neutral [40]. It was hypothesized that water could play a role in the keto-enol isomerization step which would have resulted in slightly higher activity for the direct-HDO route. Renewable feeds are known to contain alkali and alkaline-earth metals and phosphorus in form of phospholipid as contaminants. Kubicka et al tested several feedstocks with varying amounts of metals and phosphorus. They found that when alkali metals are present without their respective anion then there is a drop in the catalyst

activity and decrease in activity for direct-HDO route. With phospholipids the catalyst deactivation was so severe that it led to plugging of the reactor and pressure build-up. It was postulated that phospholipid would decompose to phosphoric acid which acts as an oligomerization catalyst for unsaturated hydrocarbons which would have accelerated the coke formation and deactivation.

3 Methods

3.1 Catalyst Preparation

The γ-Al_2O_3 (PURALOX®, Sasol) with particle size range 150–200 μm and a surface area (199m^2/g), and a pore volume (0.48 ml/g) was used as support for preparation of NiMo and unpromoted Mo catalysts. These two catalyst systems were synthesized by using a conventional impregnation method on the alumina support using aqueous solutions of the following metal precursors, $(NH_4)_6Mo_7O_{24}{\cdot}4H_2O$ (Sigma Aldrich) and $Ni(NO_3)_2{\cdot}6H_2O$ (Sigma Aldrich). In the first step of the sequential impregnation, 15 wt% Mo was added dropwise from an aqueous solution of the Mo precursor into an aqueous solution of alumina and then dried to remove water. A portion was removed at this stage and used as the unpromoted Mo catalysts for HDO experiments after calcination. Calcination was done at 450 °C with a ramp rate of 10 °C per min in air for 2 h. The second step was the loading of Ni. An aqueous solution of nickel salt was added to the aqueous solution of material prepared in the previous step and then dried to remove water. Again, this sample was calcined at 450 °C in air. These two catalyst samples were marked as Mo/Al_2O_3 and NiMo/Al_2O_3 [41].

3.2 Other materials

Oleic acid (Fluka, technical grade 90%) was employed as a feedstock in the first study. It was used as received. This technical grade OA mainly consisted of the two isomers of oleic acid (86%). The rest was other fatty acid impurities - 9-Hexadecenoic acid (palmitoleic acid) about 5%, hexadecanoic acid (palmitic acid) about 4%, tetradecanoic acid (myristic acid) about 3%, while stearic acid and eicosenoic acid were less than 1% as per the GC analysis. We will refer to these acids, other than OA, as “Other acid impurities”. The iron oleate (FeOA) complex which was employed as poison in the HDO experiments, was synthesized following a procedure reported elsewhere [42].

For the second study, stearic acid (Merck, reagent grade 95%) was used as a model compound. It contained only 1.5% tetradecanoic acid (myristic acid) impurity as determined by GC analysis. Octadecanal (stearaldehyde) and octadecanol (stearyl alcohol) were also employed in this study. Octadecanol of 99% grade was purchased from Sigma and used as is. Octadecanal was synthesized using a mild oxidizing agent (pyridinium chlorochromate) following a procedure as described elsewhere [43].

3.3 Catalytic activity measurements

All the HDO experiments in both studies were performed in a 300 ml stainless steel autoclave (Parr instruments) equipped with an internal stirrer. The reactor was equipped with a liquid sampling line to collect small aliquots (0.8-1.2 ml) during the experiment. The sampling line was wrapped with heating tape to keep it warm and prevent solidification of the samples.

Table 1: Concentrations of poison in weight ppm studied for each catalyst and experiment abbreviations (Article 1).

Poison in feed (ppmw)	**Catalyst**	
	NiMo/Al_2O_3	***Mo/Al_2O_3***
0	NiMo_0 Fe	Mo_0 Fe
20	NiMo_20 Fe	-
100	NiMo_100 Fe	Mo_100 Fe
500	NiMo_500 Fe	Mo_500 Fe
2000	NiMo_2000 Fe	-

In the poisoning study (with Fe), 1 g of catalyst and oleic acid (15 wt%) in dodecane (Sigma Aldrich) with a total volume of the reaction mixture of 150 ml was employed. A set of experiments with Mo/Al_2O_3 and $NiMo/Al_2O_3$ with different iron oleate (Fe poison) concentration was planned as given in Table 1. Poison (FeOA) was added at the beginning of the experiment. The poison concentration is reported in ppmw, i.e. milligrams of iron per weight (kg) of total liquid feed to the reactor. In Table 1; abbreviations for experiments are denoted by: (catalyst used) (concentration of poison), e.g. “NiMo_X Fe” where X is the concentration of iron in ppmw with respect to the total feed. DMDS (Sigma Aldrich) was used for the pre-sulfiding step as described elsewhere [44]. Meanwhile, a small amount of DMDS (0.1 ml) was added to the reaction mixture in each HDO experiment to maintain the sulfidity of the catalyst. Reactor conditions were kept constant for all experiments in this study - 60 bar H_2, 325 °C and with a stirring rate of 1000 rpm for 330 min. At the beginning of an experiment, first the reactor was flushed with nitrogen to remove any air, then with hydrogen. Then it was depressurized to 0.1 bar gauge and heating was switched on with a low rate (150 RPM) of stirring. After reaching the desired temperature, stirring was increased to 1000 RPM. Hydrogen was introduced at this point and this moment was considered as the start of experiment. Liquid samples were collected at progressive time intervals of – 15, 35, 55, 95, 155, 215, 275 and 330 min. At the time of liquid sampling, stirring was temporarily stopped to avoid any catalyst carryover. Fine particles of catalyst could damage the seals in the valves on the liquid sampling line. Pressure loss due to collection of liquid sample was replenished by topping up with hydrogen to maintain the same pressure throughout the experiment. Spent catalyst was recovered after the experiment after filtering with 200 ml of warm ethanol and dried for subsequent characterization. The carbon-chain (all C17 and C18 species) mole balance based on the initial feed concentration was in an acceptable range of 90–110% unless otherwise mentioned.

Table 2: Reaction conditions for the kinetic experiments

Feed component	Pressure (bar)	Temperature (C)	Feed (wt%)	Stirring (RPM)	Catalyst wt. (g)
SA	40,50,70	300	5	1000	0.4
SA	50	275,300,325	5	1000	0.4
SA	50	300	2,5,8	1000	0.4
SA	50	300	5	500,900,1000	0.4
SA, C18=O, C18-OH	50	275	5	1000	0.04

For the kinetic study, the same experimental setup was used as above, though only a 0.04-0.4 g of NiMo catalyst was used for HDO of different feeds like SA, C18=O, C18-OH and mixture of SA & C18-OH in dodecane with the same total liquid volume of 150 ml. Reaction conditions for the baseline experiment were- 5 wt% of SA, 50 bar H_2, 300 °C, stirring speed of 1000 RPM and 0.4 g of pre-sulfided catalyst. Table 2 lists all the experiments carried out in the second study with different parameters tested. Most of the protocols were kept the same as the previous study. The same conditions were used for sulfiding of the catalyst but DMDS was not added at the beginning of the reaction to avoid any side reactions. During thermal decomposition of DMDS, hydrogen is consumed while methane is produced which is an additional process that would have to be considered for the kinetic modeling. The pressure drop from sampling and pressure increase from hydrogen top-up were duly recorded at each sampling interval. Gas samples were collected at the end of the experiment. An additional baseline experiment was done to collect gas samples at 40 and 90 min intervals.

3.4 Product analysis

Liquid samples from HDO experiments were analyzed using a GC-MS equipped with a flame ionization detector (FID) (Agilent 7890-5977A). Data analysis was done using MassHunter data analysis software with NIST library. It had a non-polar HP-5 capillary column (L=30m, Dia.=0.25mm & Film=0.25 µm). BSTFA (N,O-bis(trimethylsilyl) trifluoroacetamide (Sigma Aldrich, ≥99.5%) was used to do silylation of the samples. Silylation increases the volatility and elution of oxygenate species so that peaks in the chromatogram are well separated and sharp. Calibration of the FID was done with high purity external standards of oleic acid, stearic acid, 1-octadecanol, octadecanal, octadecane, heptadecane, hexadecane, pentadecane and tetradecane. Moreover, the peaks from other minor compounds were quantified using the effective carbon number method based on the closest related calibrated compound.

The following are the formulas used in this thesis for quantities that assess the experimental results:

Conversion of oxygenates = $\left(1 - \frac{moles\ of\ oxygenates\ in\ the\ sample}{moles\ of\ starting\ oxygenates}\right) \times 100$

Yield% of C_{17}^{+} & C_{18}^{+} and minor products = $\frac{moles\ of\ product\ produced}{moles\ of\ reactant\ in\ feed} \times 100$

Initial rate of reaction = $\frac{Initial\ mmoles\ of\ oxygenates - mmoles\ of\ oxygenates\ in\ first\ sample}{time\ (hr) * wt.of\ catalyst\ (g)}$

Rate of formation of C_{17}^{+} = $\frac{mmoles\ of\ \mathrm{C17+}\ in\ first\ sample}{time\ (hr) * wt.of\ catalyst\ (g)}$

Rate of formation of C_{18}^{+} = $\frac{mmoles\ of\ \mathrm{C18+}\ in\ first\ sample}{time\ (hr) * wt.of\ catalyst\ (g)}$

Selectivity of C_{17}^{+} = $\frac{mmoles\ of\ \mathrm{C17+}\ at\ end\ of\ the\ reaction}{mmoles\ of\ \mathrm{C17+}\ \text{and mmoles of}\ \mathrm{C18+}\ at\ end\ of\ the\ reaction}$

Selectivity of C_{18}^{+} = $\frac{mmoles\ of\ \mathrm{C18+}\ at\ end\ of\ the\ reaction}{mmoles\ of\ \mathrm{C17+}\ \text{and mmoles of}\ \mathrm{C18+}\ at\ end\ of\ the\ reaction}$

3.5 Catalyst characterization

3.5.1 Nitrogen physisorption

For supported catalysts, the number of active sites depends on the surface area, and surface area is dependent on parameters like particle size and morphology, surface texturing, and porosity. Porosity and pore structure are very important factors affecting the activity of a given catalyst. Nitrogen physisorption is a phenomenon in which, when N_2 gas comes in contact with a solid surface (at 77k), a specific number of molecules are attracted to the surface of the solid by van der Waals forces. The number of physisorbed molecules depends on the relative pressure (p/p_0) of the nitrogen gas at equilibrium. N_2 physisorption was carried out at -196 °C on a Micromeritics ASAP 2010 instrument for pore structure analysis. Catalyst samples (approx. 300 mg) were degassed at 225 °C under vacuum conditions for 3h. Specific BET surface area (SBET) was calculated from the adsorption data in the relative pressure range of 0.05–0.2. The pore size distribution curves were calculated using the Barrett–Joyner–Halenda (BJH) method based on analysis of the desorption branch of the isotherm.

3.5.2 Elemental analysis

Carbon, hydrogen and sulfur content of the spent catalyst samples were determined by elemental analysis. In elemental analysis, the sample undergoes combustion at 800 °C in excess of oxygen. Then the gaseous combustion products are trapped. These gases are separated through a column and measured by a thermal conductivity detector (TCD). C and H content was determined on a CE Instruments elemental analyzer model EA111 while for S, analysis was carried out on a Fisons elemental analyzer model NA2000.

3.5.3 ICP analysis

For quantification of the metal contents (Ni, Mo and Fe), inductively coupled plasma sector field mass spectrometry (ICP-SFMS) technique was employed. The sample is dissolved in HNO_3 and digested in a microwave oven, and then fed into the instrument where the sample is ionized with inductively coupled plasma (ICP) and then quantification and separation of ions is done using a mass spectrometer. In this study, ICP analysis was carried on a Thermo Element XR instrument.

3.5.4 Temperature programmed reaction

Temperature programmed reaction of spent catalysts with hydrogen was carried out to gain insights about the effect of poison (Fe) on sulfur vacancies (CUS). An amount of 50 mg of catalyst sample was placed in a quartz tube under a continuous flow of 20 ml/min at ambient conditions. Catalyst samples compared were - (NiMo_0Fe and NiMo_500Fe). These samples were degassed in a stream of argon gas at 350 °C. Then they were cooled down to ambient temperature after which they were exposed to a stream of Ar containing 100 ppm hydrogen for 1 h. Then the concentration of hydrogen in the gas stream was increased to 400 ppm and maintained at that level for 30 min. After that, the temperature was ramped up to 800 °C at a rate of 10 °C/min during continuous dosing of hydrogen. The temperature was finally maintained at 800 °C for 30 min. The H_2 and other eluents in the outlet gas stream were monitored with a Hiden Analytical HPR 20 quadrupole mass spectrometer (MS).

3.5.5 Transmission electron microscopy (TEM)

The relative distribution of poison (Fe) with respect to active metals (Ni and Mo) was determined by TEM-EDX mapping. HAADF-STEM imaging of catalysts samples after being exposed to poison under the reaction conditions was analyzed by a FEI Titan TEM, operating at 300 kV, equipped with EDX. Samples for TEM analysis were prepared by making a suspended solution in ethanol and then letting it dry on the carbon coated copper grid at room temperature. Length of slabs and stacking degree for MoS_2 was also measured using ImageJ software. TEM-EDX mapping was done at four different spots for repeatability and for sufficiently long periods in order to stabilize the signal collection.

3.6 Kinetic modeling methods

Kinetic studies are critical to connect the microscopic picture of molecules undergoing reactions to the macroscopic picture of reaction engineering which extends to commercial scale. Needless to say, kinetics is one of the key disciplines in the field of catalysis. Even, a simple model based on power-law kinetics could predict the dependence of the individual components on the rate of a chemical process. This is critical information to predict how a reactor behaves in a given range of temperature and pressures.

3.6.1 Reactor Model

A pseudo-homogeneous ideal batch reactor was assumed for the model that comprised a set of differential equations for each component –

$$\frac{dN_j}{dt} = \sum (\gamma_{ij} r_i) W$$

Where N_j is the number of moles of component j, γ_{ij} is the stoichiometric coefficient for component j in reaction i, r_i the rate of reaction of reaction i and W is the mass of catalyst. The batch reactor was assumed to operate under isothermal conditions all the time and the rates of all reactions were considered to be dependent on the concentrations of components in the liquid phase. The liquid and gas phases were considered to be in a state of quasi–equilibrium. The compositions and densities of vapor and liquid phases were determined by calculating the vapor-liquid equilibrium (VLE) based on the Predictive Soave-Redlich-Kwong (PSRK) group contribution equation of state (EOS) by Holderbaum and Gmehling [45]. There have been other studies which have suggested PSRK EOS is most suitable for VLE estimations of similar feeds containing fatty acids for HDO reactions [46]. The PSRK critical constants and group interaction parameters were taken from literature [47]. The amount of hydrogen added to the reactor at the start of the experiment was calculated by an iterative approach using the EOS. All calculations in this kinetic study were carried out using a customized MATLAB R2014b program.

3.6.2 Reaction Equilibrium

The temperature dependence of equilibrium constants (K_{eq}) for reactions were calculated from equations with the form:

$$K_{eq} = \exp(\frac{A}{T} + B\ln(T) + CT + DT^2 + ET^3 + F)$$

Where the paramters A, B, C…etc. were calculated from standard state thermochemical properties of the components. In cases where published thermochemical properties were not available they were estimated from the Joback Method [48].

An equilibrium between octadecanal and octadecanol was considered which has been suggested by other studies as well. It could influence the selectivity between direct-HDO and decarbonation products. The rate of this reaction was multiplied by a driving force factor (β), that would approach zero as equilibrium is reached. This driving force factor was:

$$\beta = 1 - \frac{a_{C18OH}}{a_{C18=O} a_{H2} K_{eq}}$$

3.6.3 Parameter estimation for kinetic model

Reaction rate constants were expressed according to a modified Arrhenius equation:

$$k_i = k_{ref} exp\left(\frac{E_i}{R}\left(\frac{1}{T_{ref}} - \frac{1}{T}\right)\right)$$

This formulation was used to reduce the strong correlation between the pre-exponential factor and the activation energy. Thus the rate constant at the reference temperature (k_{ref}) and the activation energy (E) were the estimated kinetic parameters. The reference temperature used was 300°C, the mean experimental temperature.

For parameter optimization, the 'simulannealbnd' function in Matlab 2014b's optimization package was used to perform non-linear regression. Simulannealbnd is a global optimizer based on the simulated annealing method. The objective function of the parameter optimization was to minimize the sum of squares of the residuals (SSR) calculated from

$$SSR = \sum_{j} \sum_{i} w_i \left(y_{ij}^{exp} - y_{ij}^{sim} \right)^2$$

Where the residuals were computed from differences between the simulated (y_{ij}^{sim}) and experimentally (y_{ij}^{exp}) measured yields of component *i* from experiment *j*. The residuals for intermediate species, with lower concentrations, were typically weighted up by a factor (w_i) corresponding to the approximate ratio of average concentrations of a high concentration component (e.g. reactants and final products) to the low concentration component.

4 Results and Discussion

This thesis is based on two independent studies presented in Articles I and II. In the first study (Article I), the effect of iron Fe as poison was investigated for HDO of OA over MoS_2/Al_2O_3 and $NiMoS/Al_2O_3$. In the first study, HDO experiments demonstrated the influence of a poison (Fe) on the change in activity and selectivity of two catalyst systems. Then to elucidate the role played by Fe, spent catalysts samples were characterized using the above mentioned characterization techniques. Results from temperature programmed reaction (with H_2) and TEM-EDX analysis helped to correlate the results from the experiments. In the second study (Article II), we carried out HDO of SA at different conditions by varying parameters like – temperature, H_2 pressure, feed concentration and stirring speed. Also, reaction with other feeds like octadecanal (C18=O) and octadecanol (C18-OH) were carried out to gain a deeper understanding about the reaction scheme, and relative rates of competing reactions (e.g. decarboxylation and decarbonylation). Then, a pseudo homogeneous ideal batch reactor model, an EOS model for phase equilibrium and a kinetic model based on a proposed reaction scheme was used to predict experimental results. Results from simulations were compared to experimental results.

4.1 Fe poisoning during HDO of OA

4.1.1 HDO of OA over NiMo catalysts

A typical reaction scheme for HDO of OA, as illustrated in Fig 4, includes- firstly a fast hydrogenation of the double bond present on the long alkyl chain to produce stearic acid. Then the acid functionality is reduced to yield an aldehyde (octadecanal). Octadecanal is the common intermediate for the two possible routes of decarbonylation and direct-hydrodeoxygenation [20, 25, 40]. This scheme from stearic acid was also confirmed by experimental observations in the second kinetic modeling study. So, the carbonyl group (-C=O) exhibits tautomerism to exist in the enolic form which is saturated to form 1-octadecanol [20]. The alcohol is further deoxygenated to give unsaturated products. A number of alkene isomers were seen in the GC chromatogram which suggests that a carbon cation intermediate was involved. Alkene isomers were hydrogenated to octadecane. While for the DCOx route, oxygen is removed in the form of CO/CO2 molecules either from Octadecanal or Stearic acid to produce C17 alkenes. They are subsequently hydrogenated to form heptadecane as the final product. Selectivity from these two main routes were quantified by summing the hydrocarbons (both alkenes and alkanes) having the same carbon length. The oxygenate conversion was based on a sum of the oleic and stearic acid remaining.

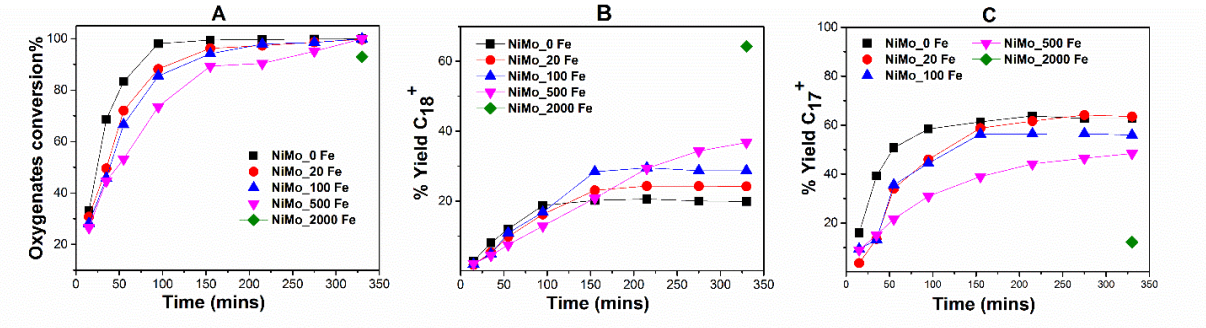

Fig 6 A, B and C: Oxygenate conversion and selectivity for major products during HDO of Oleic acid over NiMoS/γ-Al_2O_3 with varying concentrations of poison (Fe-oleate).

In Fig 6, the yield of the major products including "C17+" (sum of heptadecane and isomers of heptadecene) and "C18+" (sum of octadecane and isomers of octadecene) are depicted along with oxygenate conversion for varying concentration of poison. It can be observed in Fig 6a that complete conversion of oxygenates was achieved after varying times except for the highest poison experiment (NiMo_2000Fe), where even after 330 min, 7% of oxygenates remained in the reaction mixture. Also, note that we have only one data point for this experiment, since a poor mass balance was observed for intermediate samples. As a result, the experiment was repeated and only one sample from the reaction mixture was collected and analyzed. The deactivation effect of Fe on the catalyst is apparent by comparing the time to achieve complete oxygenate conversion with increasing poison concentration. It required 95 min to reach complete oxygenate conversion for the baseline NiMo_0 Fe experiment, while for the NiMo_500 Fe experiment it required more than three times the reaction duration. This suggests that Fe could be blocking the active metal sites. In the given experimental setup during HDO of OA on NiMo catalyst, we see from the baseline experiment that decarbonation is the preferred route while direct HDO is minor.

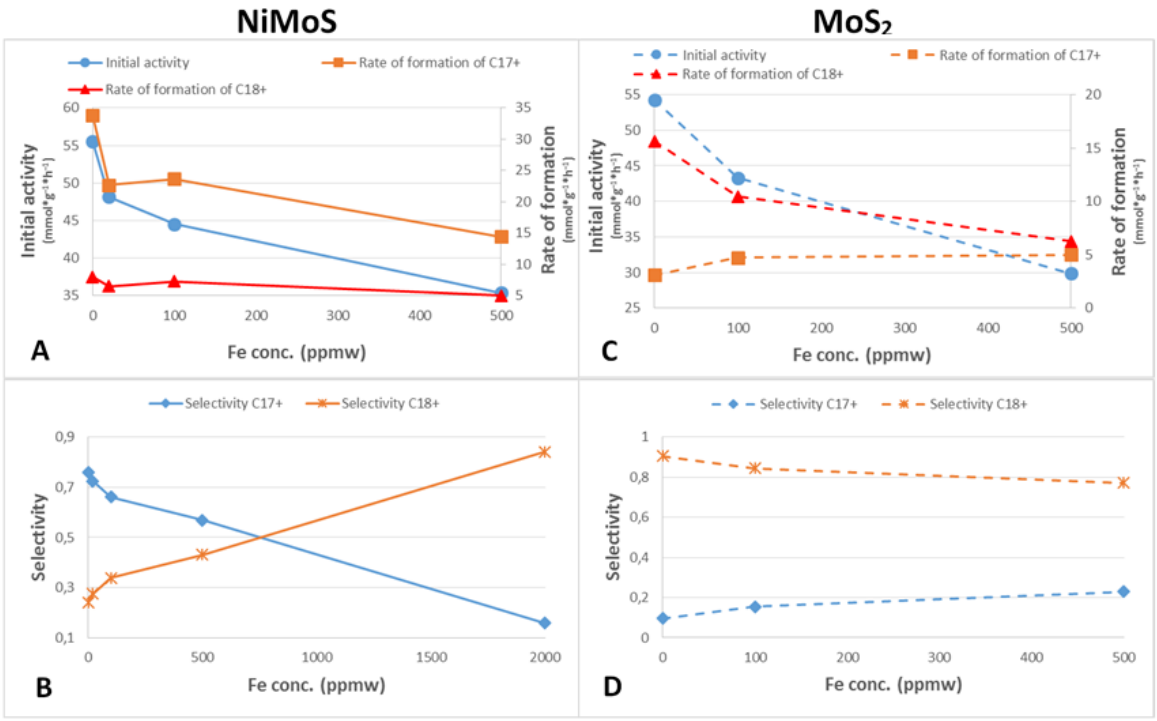

Fig 7 A B, C and D: Comparison of initial activity for oxygenate conversion and rate of formation for C17 & C18 and final selectivities (after 330 mins) for DCOx & HDO routes for different poison (Fe-oleate) concentrations with NiMoS (solid line) and MoS_2 (dash line).

In Fig 7, the initial activity of the catalyst and selectivity with the poison (Fe) concentration is compared. From Fig 6B, 6C and 7B, the effect of Fe on the selectivity of products is evident. With increasing Fe concentration, the selectivity for C17+ decreases while C18+ formation becomes the preferred route at the Fe concentration of 2000 ppmw. From comparing the baseline experiment with the NiMo_500 Fe experiment, it can be seen that the selectivity for the DCOx route has decreased from 0.76 to 0.57 (Fig 7B). Consequently, there is an increase in the selectivity for C18+ products with increased poison. We could see from the results that the effect due to deactivation of the catalyst on the DCOx route is more than compared to the direct-HDO (in Fig 7A). It should be mentioned that in a refinery setup, the direct-HDO product is often preferred as it retains more carbon atoms in the valued products and represents higher carbon yield [20]. Also, the consumption of hydrogen in these two routes is different. So if selectivity and activity of the catalyst is changing due to a poison, then it could have a negative impact on the product yield.

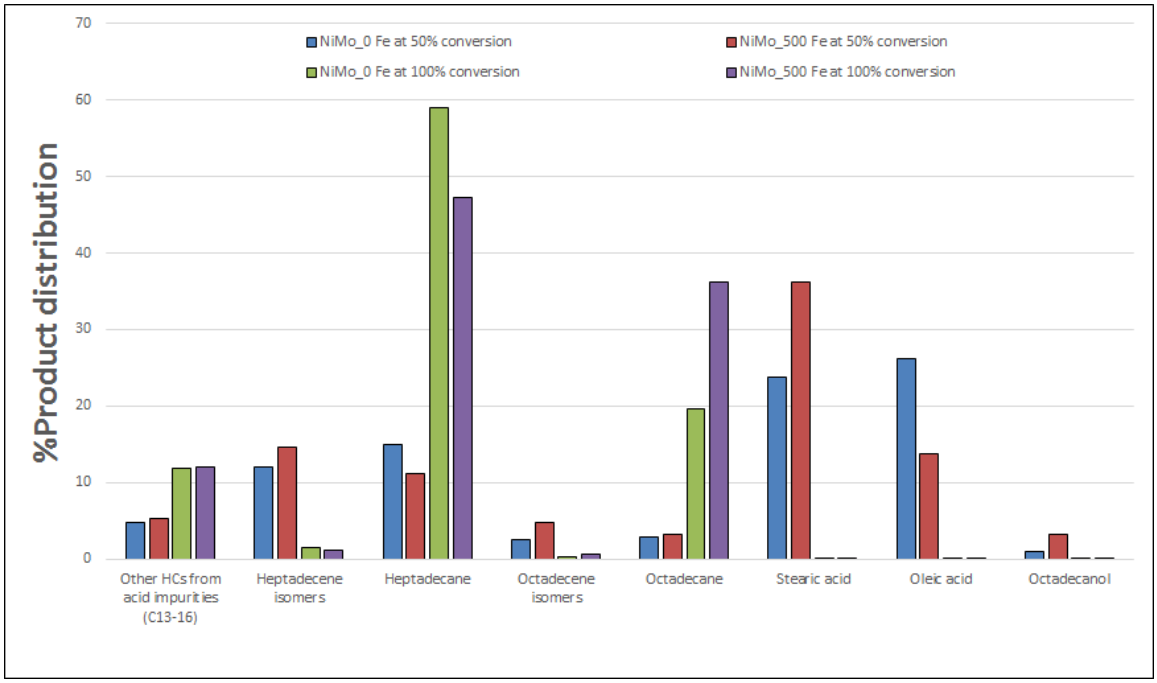

Fig 8: Product distributions for NiMo catalyst with no poison (NiMo_ 0 Fe) and high poison (NiMo_500 Fe) at 50 and 100% oxygenate conversion respectively. Results at 50% conversion interpolated from experiments.

The product distributions for NiMo_0 Fe and NiMo_500 Fe experiments at 50 and 100% oxygenation conversion are compared in Fig 8. Here, the values from the experimental data were interpolated to estimate the amounts of the respective components at 50% conversion. For both the catalyst systems, complete oxygenate conversion was achieved within 330 mins. Other acid impurities accounted for around 12% yield of products for both cases at 100% conversion. This also suggests that introduction of Fe did not enhance cracking with the NiMo catalyst at the given reaction conditions. There was an interesting observation regarding the alkene/alkane product ratio. It seems that hydrogenation capability of the active sites depleted with the addition of Fe. For both C17 and C18 products higher alkene/alkane ratios were observed even at the same conversion with increasing Fe. This is well in accordance with previous studies where it is postulated that the conversion of alkenes is delayed until most of the oxygenates are converted, since they bind very strongly to the active sites. It is evident from Fig 6 that all reactions are slowed down due to presence of Fe. In Fig 8, at 50% conversion, SA is 12% higher for the experiment with Fe (NiMo_500 Fe) when compared to the baseline experiment. Also, other intermediates like octadecanal and octadecanol were found to go via a larger maxima for the poisoned experiment.

4.1.2 HDO of OA over Mo catalysts

The unpromoted molybdenum catalyst was tested since the shift in selectivity with NiMo discussed in the above section was peculiar. Therefore HDO of OA was carried out on MoS_2 at different Fe concentrations, as shown in Table 1. Fig 9 A, B and C compare the three experiments with varying Fe concentration (0, 100 and 500 ppmw) for oxygenate conversion and for selectivity of the two main routes. The reaction chemistry was similar to the one seen with Ni promoted catalysts with two main differences. On the MoS_2 surface, much larger amounts of octadecanol

were observed during the course of the reaction. Here, direct-HDO was found to be the major route, unlike for the Ni promoted catalyst. Irrespective of the Fe concentration in the feed, it was clear that selectivity is in favor of C18+ products (Fig 7D and 9B). From Fig 9B, the conclusion could be drawn that MoS_2 active sites have a higher tendency for hydrogenation reactions, which results in a selectivity of more than 80% for the direct-HDO route. This characteristic of Mo based catalysts has been reported in other studies as well [49]. A similar trend of decrease in activity could be observed with the increased Fe in the feed, where a longer duration is required to reach complete conversion of oxygenates. From Fig 7C, it could be seen that there is a drop in the initial activity, so clearly Fe seems to be blocking the active sites on the catalyst surface. It has been reported that for such catalyst systems activity order is NiMo>Mo>Ni on alumina [30]. The same order can be observed from the experimental results in this study.

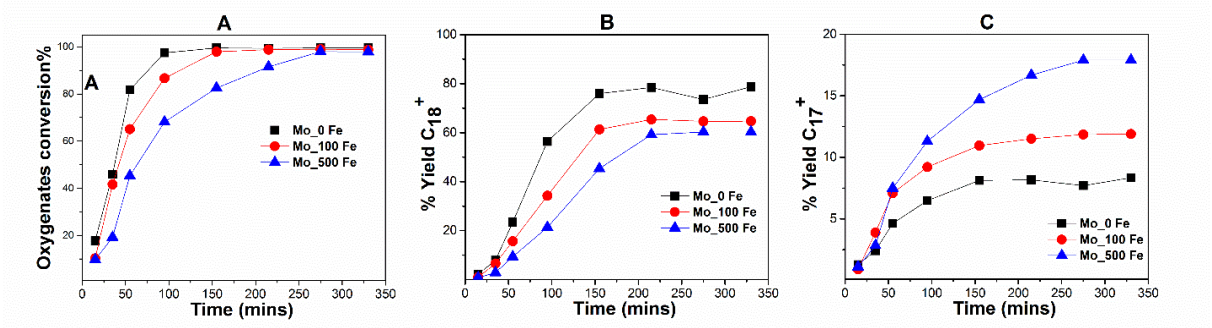

Fig 9 A, B & C: Selectivity of major products during HDO of Oleic acid over $MoS_2/\gamma\text{-}Al_2O_3$ with varying concentrations of poison (Fe-oleate).

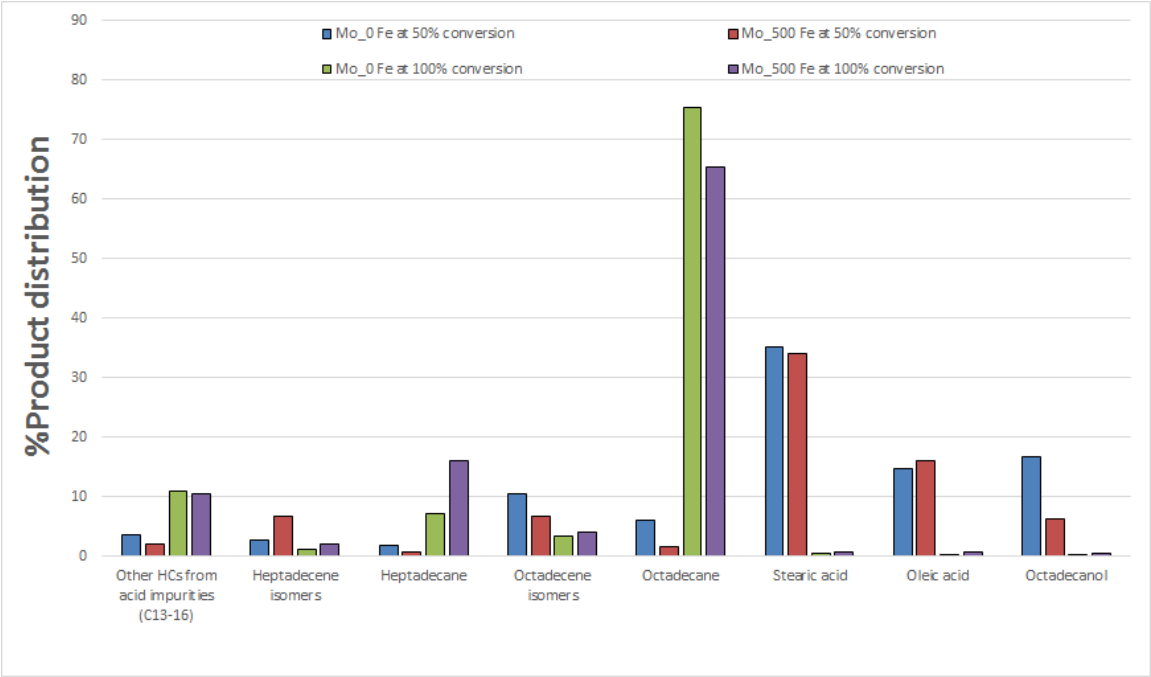

Fig 10: Product distributions for MoS_2 catalyst with no poison (Mo_ 0 Fe) and high poison (Mo_500 Fe) at 50 and 100% oxygenate conversion respectively. Results at 50% conversion interpolated from experiments.

By comparison of the two catalysts systems, the drop in activity for MoS_2 was larger (44%) than that of NiMoS (36%). The promotional effect of Ni on molybdenum catalysts have been explained

mechanistically with the reasoning that at the Ni promoted sites, the antibonding S-metal d states are below the fermi level due to the weakening of the bond between S-S on the edge. The promoting effect of Ni is due to the weakening of the metal-sulfur bond, which results in the creation of more sulfur vacancies, hence higher activity. The selectivity trend observed in this catalyst (MoS_2) was opposite to the one seen above for NiMoS. When Fe concentration was increased from 0 to 500, a drop from 80 to 60% was recorded for yield of products via direct-HDO i.e. C18+ hydrocarbons. On the other hand, yield of heptadecane and its isomers increased from 8 to 18% during the same range of Fe concentration. Fig 7 presents the same results in terms of selectivity with a plunge in the C18+ products with a modest jump in the decarbonation route products. Fig 10, compares the product distribution for the unpromoted molybdenum catalyst for 0 and 500 ppm Fe at 50 and 100% oxygenate conversion. The impact of Fe on the hydrogenation activity of the catalysts is evident from the increased alkene/alkane ratio. At 50% conversion, the alkene to alkane ratio for 0 and 500 ppm experiments was 1.5 and 10.4 respectively for the decarbonation route products while that for C18 products it was 1.8 and 4.4 for Mo_0 Fe and Mo_500 Fe experiments respectively. Higher amounts of oxygenates present were observed in the reaction mixture at the same time point for MoS_2, compared to that of the NiMoS catalyst. This implies that the impact of Fe poison has a larger influence on the Ni promoted catalyst, though in absolute terms, the unpromoted catalyst lost two-third of its activity.

4.1.3 Catalyst deactivation and characterization

To further comprehend the change in activity and selectivity of these two catalyst systems, extensive characterization of the samples was carried out. Table 3 displays the textural and compositional properties of both fresh and spent catalyst samples. In a patent study, it has been suggested that a renewable feed containing Fe species could lead to a rapid increase in the pressure drop due to reactor plugging [50]. The surface area and pore volume decreases due to coke formation and irreversible adsorption of certain species during the reaction. As evident from Table 3, both the surface area and pore volume dropped by 23 and 16% respectively for the NiMo_Fe catalyst compared to the fresh sample, while much less of a drop was observed for the baseline experiment (6 and 7%). This decrease is substantial, considering it was only a short HDO experiment of 330 min. Thereafter, elemental analysis was carried out to estimate the carbon content of the spent catalysts. Coking was quite low (0.76 to 1.3 wt%) for all the catalyst samples, except for NiMo_2000 Fe where it was 3.5 wt%. However, that could be explained by the fact that the conversion of oxygenates was not completed by the end of the experiment. Since these molybdenum based catalysts have an active phase in sulfided form, we looked into the sulfur content of the recovered catalyst from different HDO experiments. On the basis of calculations, the sulfur content of the MoS_2 and NiMoS catalysts would need to be 6.1 and 7.2 wt% respectively to achieve complete sulfidation of the active phase. However, from Table 3, it could be seen that the sulfur content was in the range of 6-11 wt%, which suggest that there was not much loss in the sulfur from the active phase. Slightly higher amounts of sulfur present could be attributed either to loosely bound sulfur species on for example the support or some uptake by Fe to form FeS-like compounds.

Table 3: Textural properties and elemental content of sulfur and carbon on fresh and recovered catalyst samples.

	BET surface area [m^2g^{-1}]	Pore Volume [cm^3g^{-1}]	Average Pore Size [Å]	S [wt%]	C [wt%]
γ-Al_2O_3	199	0.48	97.6	<0.1	0.1
NiMo (fresh)	141.5	0.31	87.6	<0.1	0.04
Mo (fresh)	154.5	0.33	88.2	<0.1	0.04
NiMo_0 Fe [a]	131.3	0.29	86.6	8.3	0.9
NiMo_20 Fe[a]	-	-	-	6.9	0.76
NiMo_100 Fe[a]	-	-	-	7.7	1.17
NiMo_500 Fe[a]	118.9	0.24	80.8	7.6	0.72
NiMo_2000 Fe[a]	-	-	-	10.9	3.52
Mo_0 Fe[a]	144.7	0.31	87.1	6.0	1.1
Mo_100 Fe[a]	-	-	-	5.8	1.3
Mo_500 Fe[a]	132.3	0.26	81.7	5.8	1.6

[a] after 330 min of HDO reaction

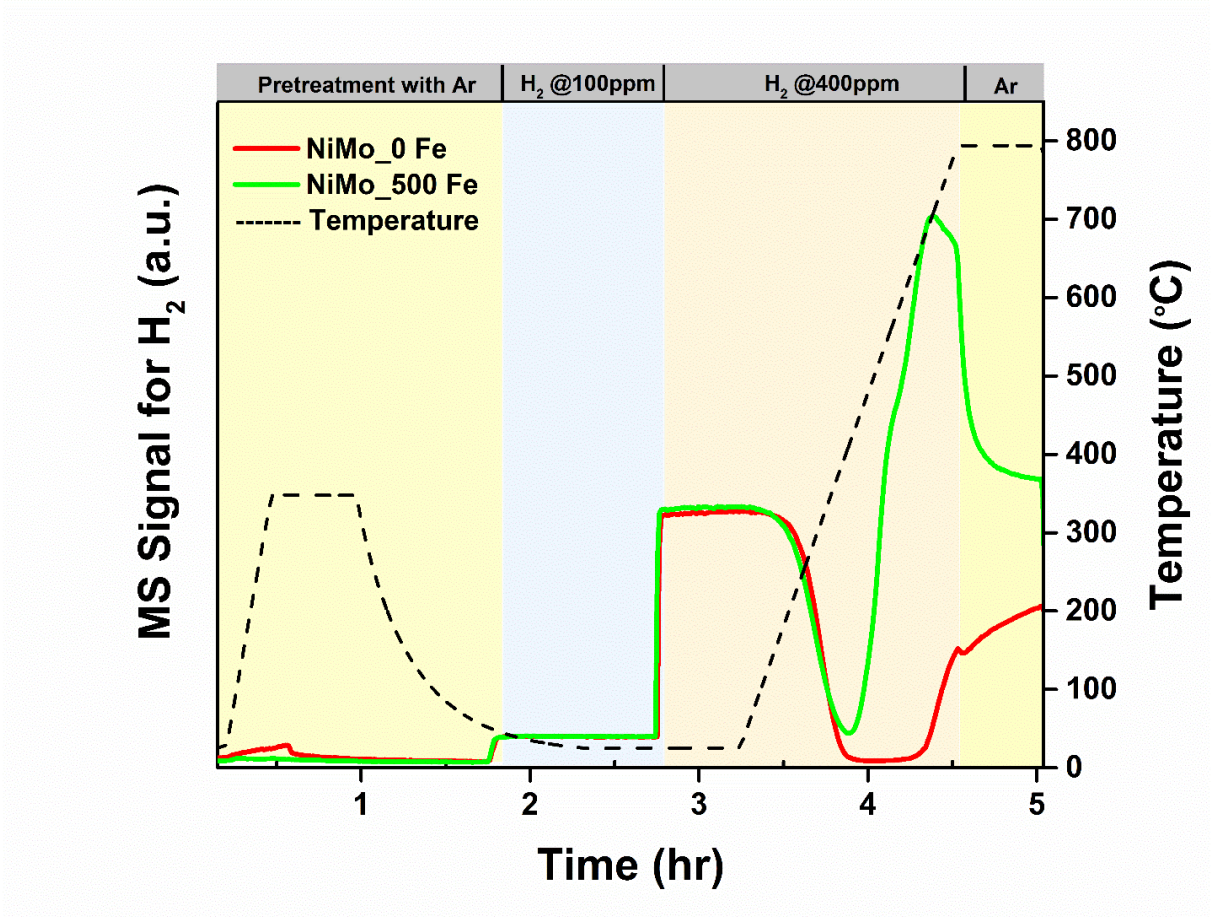

Fig 11: Pretreatment and H_2 temperature programmed reaction on recovered catalyst samples NiMo_0 Fe and NiMo_500 Fe.

Results of temperature programmed reaction with hydrogen are depicted in Fig 11. In this analysis, spent catalyst from NiMo_0 Fe and NiMo_500 Fe experiments were used. There was a negligible hydrogen adsorption at ambient temperature. It started only at a higher temperature of about 200 ˚C. After further increasing the temperature, the NiMo_500 Fe sample desorbed approximately the same amount of hydrogen starting at around 400 ˚C. Hydrogen was more reactive with the sample from the baseline (NiMo_0 Fe) experiment, as many sulfur containing species like H2S were observed by the mass spectrometer. This suggests that the labile sulfur was present much more in the absence of Fe poison. As explained in Section 2.2 above, for TMS catalyst systems, the creation of sulfur vacancies are the first step of their catalytic cycle. Sulfur vacancies have a direct correlation to the activity of such catalyst systems. Fe salts are known to be moderately oxidative in nature, so it could be postulated that the active sulfide phase has been oxidized and rendered inert for reaction with hydrogen even at higher temperatures by the Fe poison.

Table 4: ICP analysis results of fresh and recovered catalysts and liquid phase following reaction.

	Atomic ratio		**Liquid Phase**
	Ni/Ni+Mo	**Fe/Fe+Ni+Mo**	**Fe (mg/kg)**
NiMo (fresh)	0.36	<0.01	-
Mo (fresh)	-	<0.01	-
NiMo_0 Fe	0.37	0.01	<0.2
NiMo_20 Fe	0.36	0.05	<0.2
NiMo_100 Fe	0.36	0.07	<0.2
NiMo_500 Fe	0.37	0.28	<0.2
NiMo_2000 Fe	0.37	0.57	<0.2
Mo_0 Fe	-	0.01	<0.2
Mo_100 Fe	-	0.09	<0.2

In Table 4, the results from the ICP analysis of fresh and spent catalyst samples are shown. The liquid phase after the HDO experiment was also analyzed. Fresh catalyst samples – MoS_2 had 9.2 wt% of Mo and NiMoS had 3.3 wt% of Ni and 9.3 wt% of Mo respectively. Atomic ratio for Ni/Ni+Mo was constant for fresh and spent catalyst, which indicates that there was no leaching of metal from the catalyst, and thus no reactions in the homogeneous regime. In Table 4 it could also be observed that no Fe was detected in the reaction mixture (liquid phase), which confirms that all Fe uptake was by the catalyst. In case of the Alumina_500 Fe experiment, most of the Fe remained in the liquid phase. These results allow us to propose that the Fe is being deposited on or near the metal centers of these catalyst. It could be postulated that the Fe deposition is related to the catalytic activity. When Fe oleate complexes are adsorbed at the catalytic sites, the oleate ligand is deoxygenated while Fe is deposited at or near the active sites. This is in accordance to that observed for hydrodemetallisation (HDM) during hydrotreating of fossil feeds, where the metals present in petroporphyrins like V and Ni are deposited at the active catalytic sites [51].

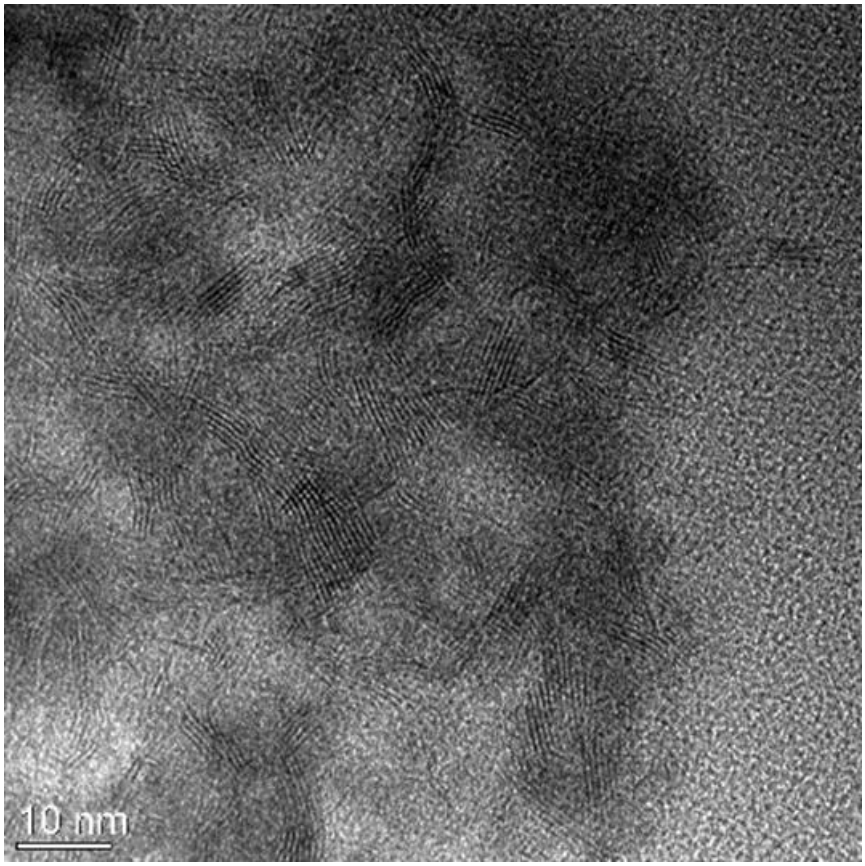

Fig 12 HR-TEM image of catalyst recovered after 330 mins of HDO (NiMo_500 Fe) experiment.

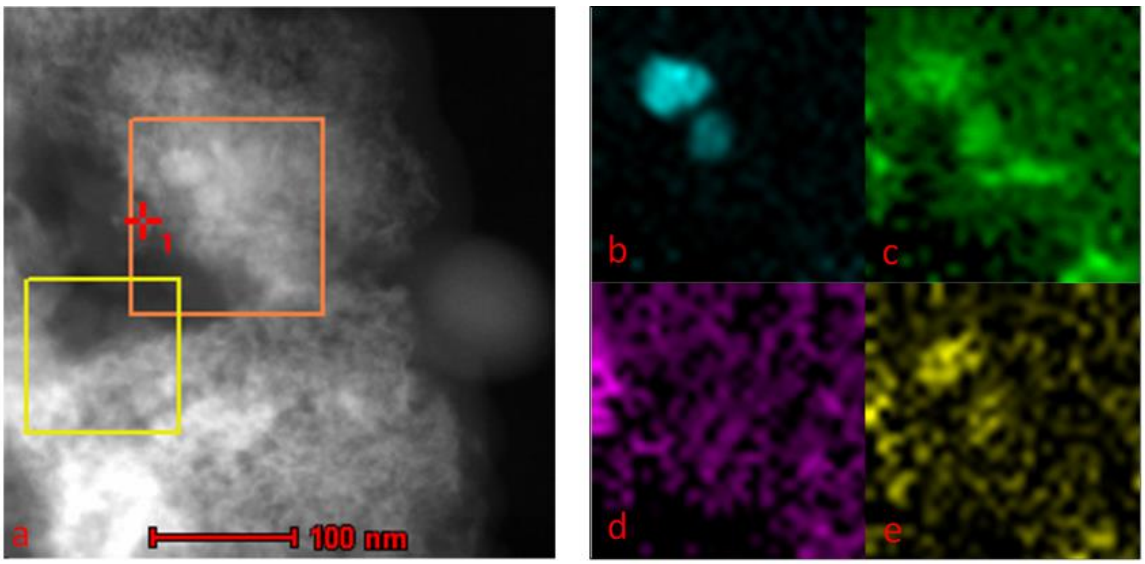

Fig 13 (a) HAADF-STEM image NiMoS recovered after 330 mins of HDO (NiMo_500Fe) experiment and corresponding EDX mapping according to elements: (b) nickel (c) iron (d) molybdenum and (e) sulfur.

TEM was employed to analyze the morphological structure of the MoS_2 slabs and dispersion of the active metal centers. Moreover, Fe poisoned catalyst samples were analyzed with TEM-EDX mapping to determine the distribution of Fe relative to Ni and Mo. Fig 12 shows an HR-TEM image of the catalyst recovered after 330 mins of HDO (NiMo_500 Fe experiment). Fig 13 depicts the

EDX mapping of the same sample for elements: nickel, iron, molybdenum and sulfur. The edge planes of the MoS_2 slabs are clearly seen which are oriented in line with or at a small angle from the electron beam in Fig 12. Moreover, the MoS_2 slabs in NiMo_500 Fe samples seem to be blurry and less distinct. This could be due to oxidation by Fe salts. This may suggest that Fe poisons promote oxidation and prevent the resulfiding of the MoS_2 phase. This theory is in concurrence with the results shown for temperature programmed reaction with H2 in Fig 11, where the spent catalyst in absence of Fe was observed to form H2S to a much greater degree than the catalyst poisoned by Fe. In the EDX elemental maps of Fig 13, the section inside the orange square was scanned for a long duration to determine the distribution of Fe, Ni, Mo and S. It is interesting to find that the distribution of Fe was closely overlaying on the signals from Ni, although Fe is present on other areas as well. This suggest that Ni promoted sites (NiMoS) would have been affected more compared to the base catalyst by Fe poisoning during HDO of Fe oleate. There are Ni rich sites on NiMoS catalyst as well the sites where Ni is absent. Ni-rich sites are selective for decarbonation while sites where Ni is scare would act like the MoS_2 phase which favors the direct-HDO route. Since, Ni-rich sites would be affected more due to Fe poisoning, then decarbonation activity selectively decreases and effectively direct-HDO is favored. We could also extend the possibility of formation of FeMo phase with the fact that Fe is a weaker promotor, compared to Ni, to enhance DCOx route. It has been shown in previous studies that Fe is a weaker promotor for HDS catalysts [52]. Thus, it is probable that Fe could have a weak promotional effect for HDO reactions, if the deposited Fe can partially form a FeMo phase.

4.2 Kinetic study for HDO of SA

4.2.1 Kinetic experimental results

A set of experiments were planned for the development of the kinetic model (see Table 2). Stearic acid, octadecanal, octadecanol, isomers of heptadecene and octadecene, heptadecane and octadecane were the common species observed in the liquid phase of these experiments. These following abbreviations were used for the given components - “Stearic acid – SA”, “Octadecanal – C18=O”, “Octadecanol – C18-OH”. Saturated and unsaturated isomers of C17 and C18 molecules were lumped together and represented by “C17+” and “C18+”. There were a few other compounds observed in the liquid phase which were less than 1% of the C-mole balance and thus ignored. These involved myristic acid, tridecane, tetradecane and stearyl stearate. Reaction schemes proposed by different research groups can be broadly divided into two groups, one in which C18-OH is the intermediate [53, 54] and the other in which C18=O is proposed to be the intermediate after catalytic reduction of SA [16, 20, 40]. Therefore, we carried out HDO experiments employing the intermediates like octadecanol and octadecanal to illustrate and confirm the overall reaction scheme for HDO of SA. Gaseous samples were analyzed and CO, CO2 and CH4 were detected in the gas samples. Decarbonylation and decarboxylation steps during HDO of SA would yield CO and CO2 respectively. However, these could be formed from one another by the water gas shift (WGS) reaction as well. Table 5 presents the results from the gas analysis. These results also helped to establish the reaction scheme for HDO of SA.

Table 5: Concentrations of carbon containing compounds in dry gas at varying reaction time or at the end of the experiment (final).

Feed component	Time (min)	Pressure (bar)	Temp(°C)	Catalyst wt. (g)	CO (mol%)	CO_2 (mol%)	CH_4 (mol%)
SA	40	50	300	0.4	1.48	0.10	0.08
SA	90	50	300	0.4	1.78	0.49	0.18
SA	180 (final)	50	300	0.4	0.88	0.83	0.54
C18-OH	270 (final)	50	275	0.04	0.00	0.00	1.01
C18=O	270 (final)	50	275	0.04	0.58	0.02	0.04

4.2.1.a HDO of Octadecanol (C18-OH)

HDO of C18-OH was carried out at lower temperature and catalyst-to-feed ratio to monitor the conversion of reactants and formation of intermediates and products. The reaction conditions were as follows; 50 bar and 275 °C with 0.04 g of catalyst. At the end of the experiment i.e. 270 min, slightly more than half (53%) of the initial octadecanol molecules had reacted. The product distribution in the liquid phase was 51% of C18+ and 1.2% of C17+ hydrocarbons. Fig 14 depicts the change in the concentration of these species. Direct-HDO was found to be the major preferred route and the selectivity for C18+ hydrocarbons was 98%. The conversion of octadecanol and the formation of C18+ products was almost linear with time. Unsaturated hydrocarbons were the intermediates formed during the dehydration of octdadecanol, subsequently hydrogenated to yield C18 alkanes. A small amount of C18=O was also observed from GC analysis of the liquid products. It suggests a minor formation of octadecanal from octadecanol. The presence of small amounts of aldehyde explains the low final yield of C17+ products of only 1.2%, which would have formed from the decarbonylation route. In the gas phase results, methane was the main carbon-containing component in the gas sample collected at the end of the experiment, while carbon oxides were in traces. Therefore, it could be concluded that C18-OH is the only intermediate for the direct-HDO route in a reaction scheme for HDO of SA over NiMo catalysts.

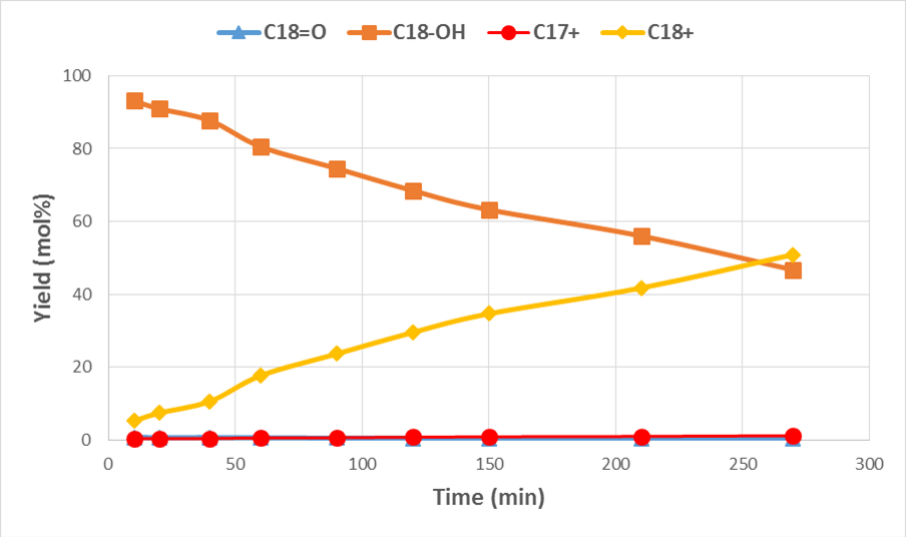

Fig 14: HDO of Octadecanol (C18-OH) at 275°C, hydrogen pressure 50 bar, feed 5 wt% C18-OH, catalyst mass 0.04 g, stirring rate 1000 rpm. Symbols are experiments, curves indicate trends.

4.2.1.b HDO of Octadecanal (C18=O)

HDO of Octadecanal (C18=O) was carried out at the same reaction conditions as above due to its high reactivity - 50 bar and 275 °C with 0.04 g of catalyst. As mentioned in Section 4.2.1, a few research studies suggest that HDO of SA proceeds via C18=O [16, 20, 40]. However, this has not been experimentally established since it has been observed only in trace amounts. Also, there is a lack of clarity about the contribution of decarboxylation and decarbonylation routes to yield C17+ hydrocarbons in the existing literature. Fig 15 depicts the concentration profile of C18=O, C17+ and C18+ during the HDO of C18=O. Octadecanal reacted at a fast rate such that it achieved 100% conversion in just 150 minutes. The formation of C17 hydrocarbons occurred quite fast as it attained a yield of 14% in the first hour of the experiment and remained constant thereafter. It is evident from Fig 14 and 15 that the selectivity for the direct-HDO route is higher with C18=O as feed compared to starting SA as feed. The sum of the final yields of C18-OH and C18+ could be regarded as the total selectivity for direct-HDO route when the conversion is not complete. When starting with C18=O feed (Fig 15) and for SA feed (Fig 16) at same conditions (275°C and 50 bar) the contribution of direct-HDO were 85% and 73% respectively. The yield of octadecanol attained a maxima of 60% at 90 min and reacted very slowly afterwards. In the gas phase (refer Table 5), the major fraction was found to be CO, while CO_2 was detected in traces. This also validates that the most of the C17+ was likely formed from the decarbonylation route.

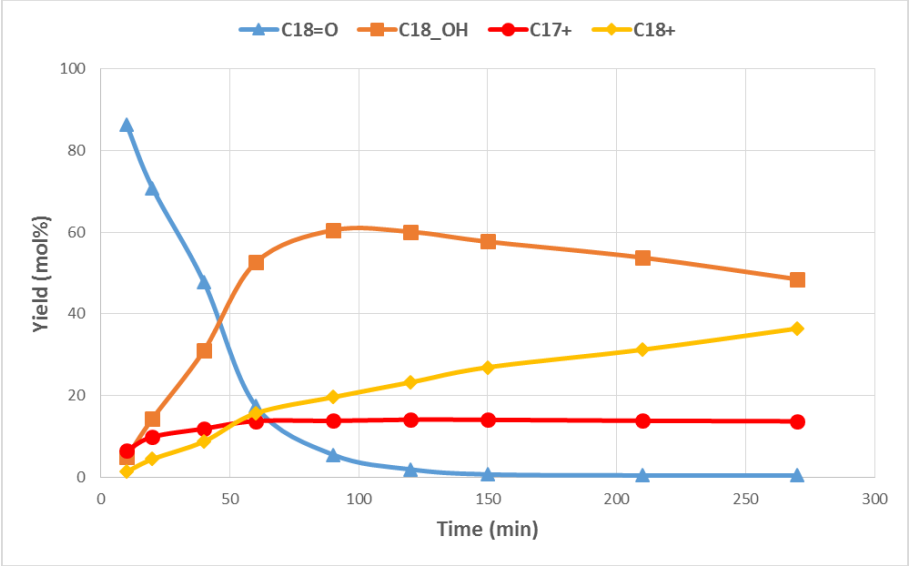

Fig 15: HDO of Octadecanal (C18=O) at 275°C, hydrogen pressure 50 bar, feed 5 wt% C18=O, catalyst mass 0.04 g, stirring rate 1000 rpm. Symbols are experiments, curves indicate trends.

4.2.1.c HDO of Stearic acid (SA)

A series of HDO experiments with SA as feed component over a range of temperature (275-325 °C), pressure (40-70 bar hydrogen), feed concentration (2-8 wt%) and stirring rate (500-1000 rpm) were carried out (see Table 2). Fig 16 represents the effect of temperature on the concentration profile of different molecules during the HDO reaction. It is evident that with the increase in temperature the rate of conversion of SA increased drastically. Time taken to achieve almost complete conversion of SA was 90, 120 and 180 minutes at 275, 300 and 325 °C respectively. Intermediates were octadecanal and octadecanol, as expected. Lower temperature resulted in a higher maxima concentration for the alcohol species with a typical concentration profile for an intermediate. Octadecanol went up to 44% at 275 °C while only 15% at 325 °C. The same effect was reflected in the selectivities for C17+ and C18+ hydrocarbons. The decarbonation route was preferred at the higher temperature. From the gas phase analysis (refer Table 5), the amount of CO during the initial time period of the experiment (at 40 and 90 mins) was much higher. The amount of CO went down as it was reduced to CH4 via methanation.

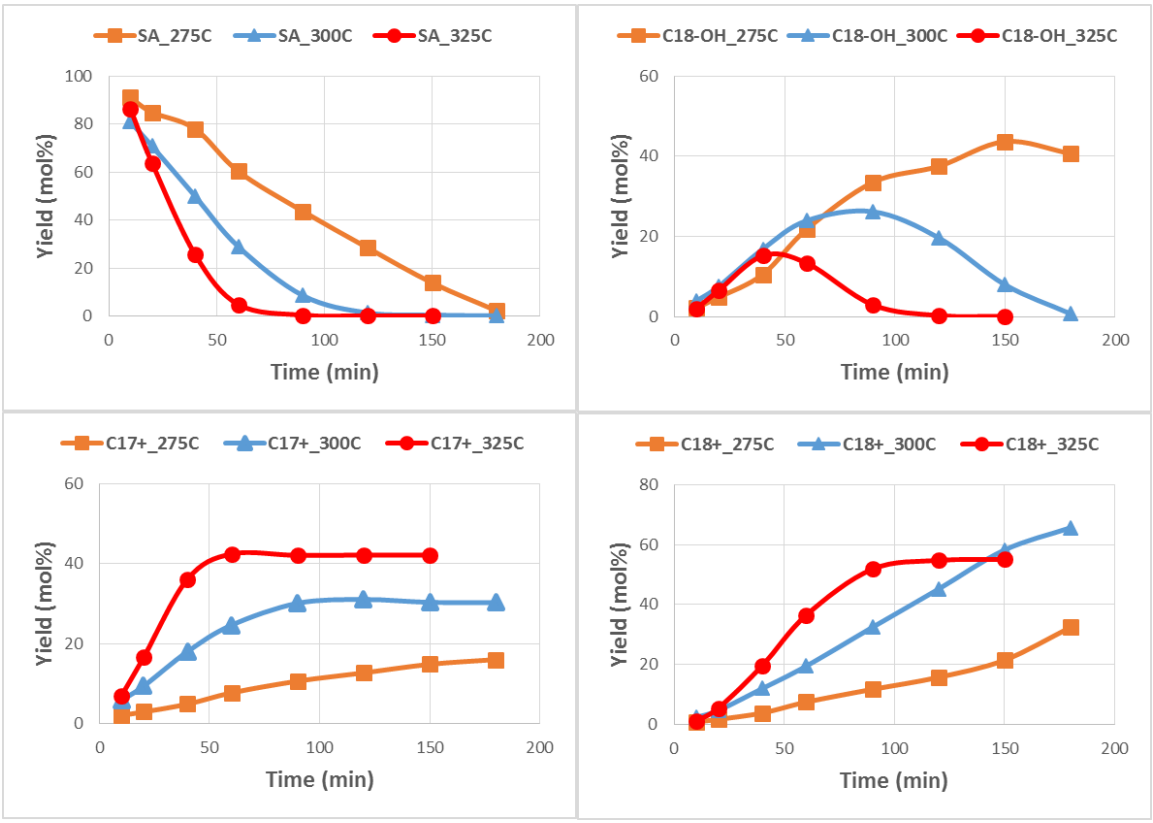

Fig 16: Temperature effect on HDO of stearic acid (SA) at hydrogen pressure 50 bar, feed 5 wt% SA, catalyst mass 0.4 g, stirring rate 1000 rpm. Symbols are experiments, curves indicate trends.

Fig 17 shows the results from experiments with varying hydrogen pressure (40-70 bar). It could be seen that the initial rate of decrease in yield of SA had a mild dependence on the H2 pressure. However, it took approximately the same amount of time (120 mins) to achieve complete conversion of SA, irrespective of the H2 pressure. However, as expected, higher pressure favored the direct-HDO rote since hydrogen is required at different steps along this route. Selectivity for the decarbonation route dropped from 38 to 23% while for the direct-HDO it increased from 58 to 73% as H2 pressure varied from 40 to 70 bar.

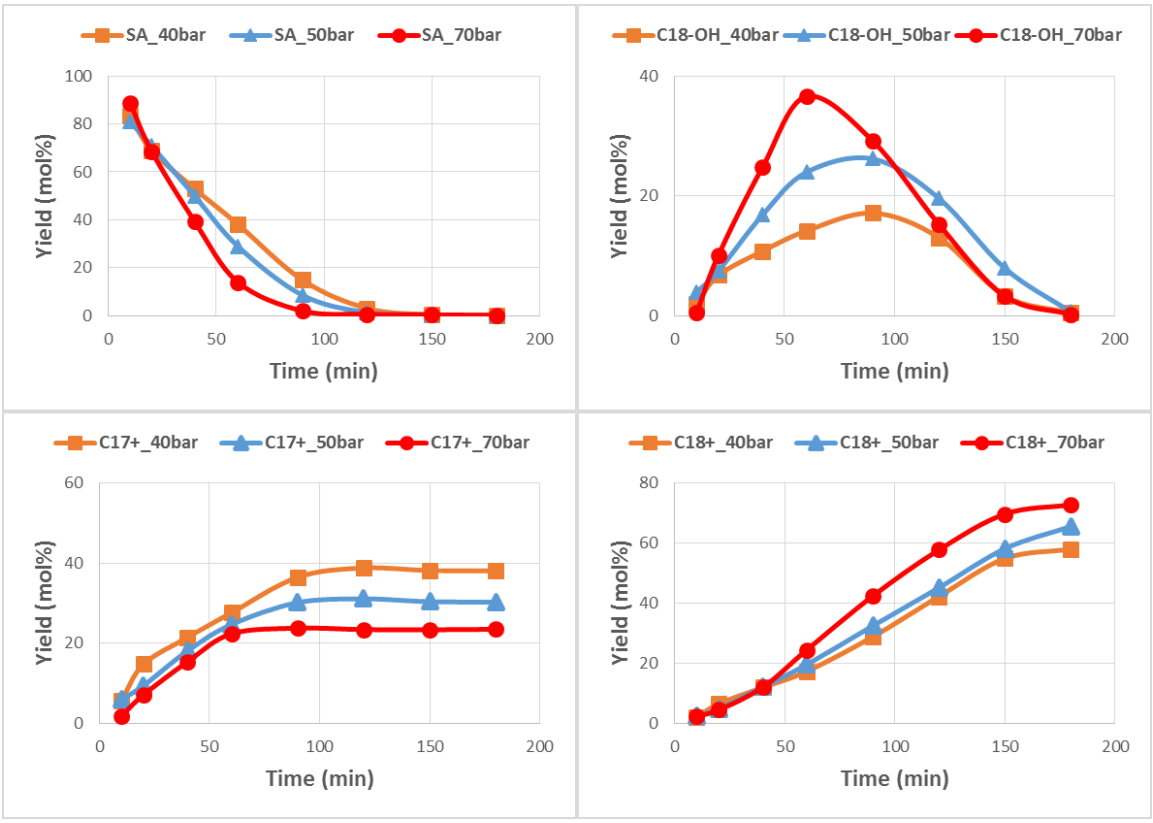

Fig 17: H_2 pressure effect on HDO of stearic acid (SA) at 300°C, feed 5 wt% SA, catalyst mass 0.4 g, stirring rate 1000 rpm. Symbols are experiments, curves indicate trends.

The effect of stirring rate in the range of 500-1000 RPM on HDO of SA has been showcased in Fig 18. There was not much difference in the products profiles for SA, C18-OH, C17+ and C18+ between 900 and 1000 RPM experiments. This suggests that the external mass limitations were absent at these high mixing rates. However, there were appreciable differences in the yield profile for the 500 RPM experiment. Octadecanol formed was much less (only 12%) when compared to higher stirring rates. This resulted in higher selectivity for C17+ products at lower stirring. It could be visualized that the transfer of hydrogen from gas to liquid to catalyst surface was restricted at low stirring rate (500 RPM). This resulted in low availability of hydrogen on catalyst surface, which therefore suppressed the direct-HDO route which requires more hydrogen per mole of fatty acid. It could be concluded that a stirring rate of c.a. 1000 RPM was sufficient to keep the liquid phase saturated with hydrogen throughout. It has been reported in the open literature that for similar reactor setups, stirring speeds of 1000 RPM or more are enough to avoid any limitations of external mass transfer for similar experimental conditions [16, 55].

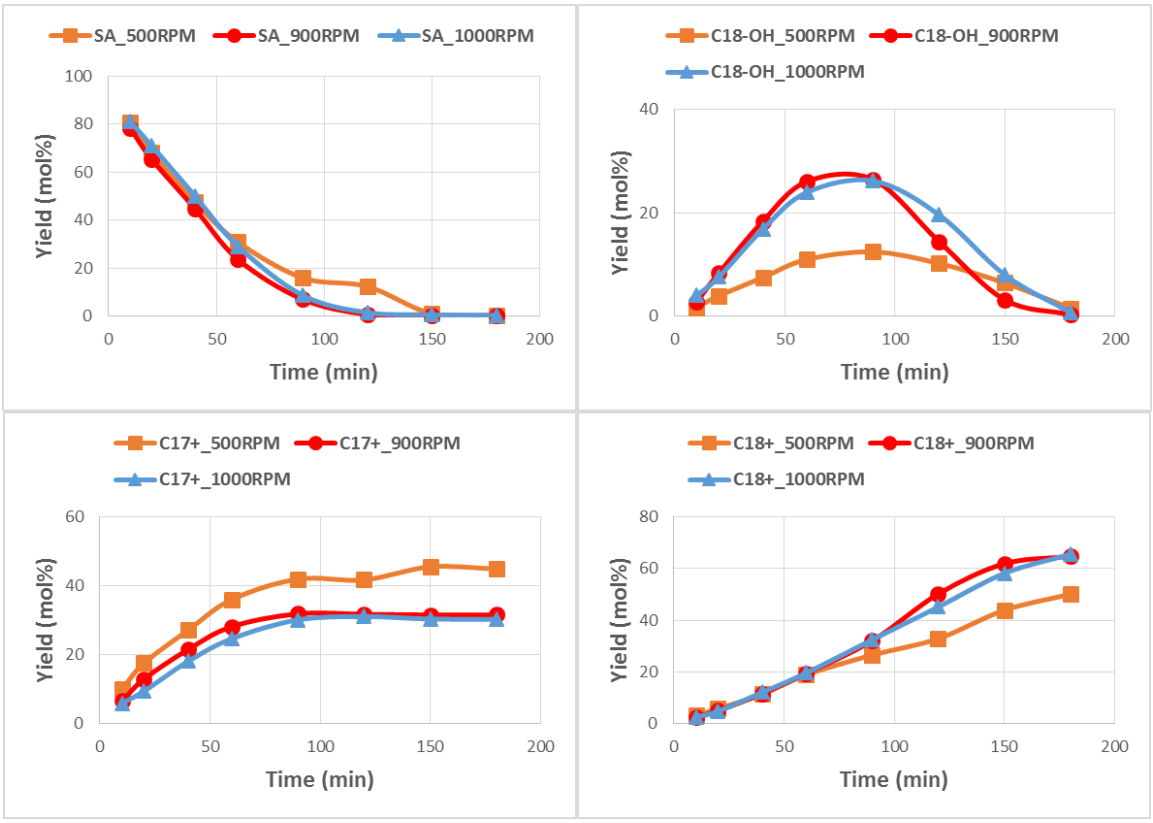

Fig 18: Stirring rate effect on HDO of stearic acid (SA) at 300°C, hydrogen pressure 50 bar, feed 5 wt% SA, catalyst mass 0.4 g. Symbols are experiments, curves indicate trends.

The influence of initial feed concentration during HDO of SA was tested for 2, 5 and 8 wt%. As shown in Fig 19, the rate of conversion of SA is higher at lower feed concentration. The concentration profile of SA indicates that the reaction with respect to SA is not first order, but instead less than unity. The duration to reach complete conversion was different for the 2, 5 and 8 wt% experiments. Initial feed concentration also had an influence on the selectivities of C17+ and C18+ products. The inhibiting effect of SA are illustrated in Fig 20. These results are from the baseline experiment with 5 wt% SA as feed, temperature 300°C hydrogen pressure 50 bar, catalyst mass 0.4 g, and stirring rate 1000 RPM. In Fig 20, products and intermediate yields are plotted against SA conversion. There is a rapid increase in the formation of C18+ products from 32 to 66% while C17+ products have plateaued at 30% at around 70% conversion. Also, there was a sudden increase in the conversion of the intermediate (C18-OH) once there was less SA remaining in the reaction mixture.

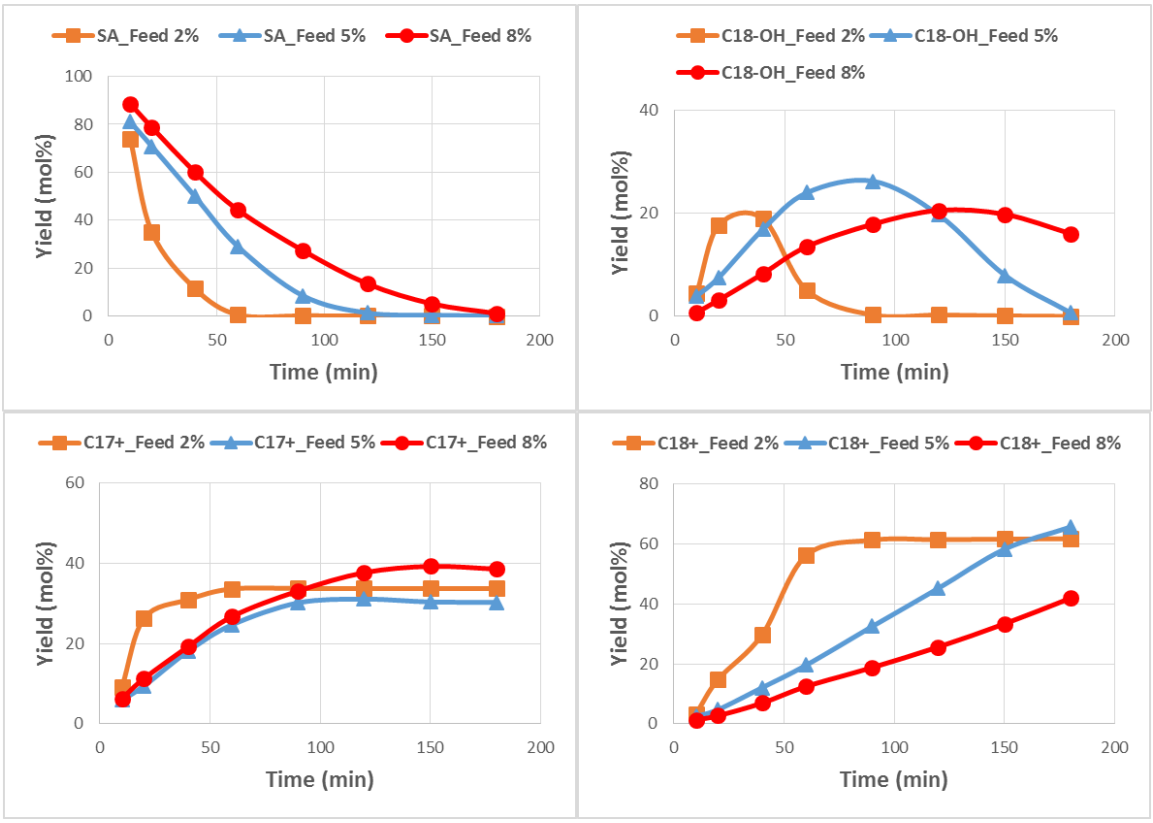

Fig 19: Initial feed conc. effect on HDO of stearic acid (SA) at 300°C, hydrogen pressure 50 bar, catalyst mass 0.4 g, and stirring rate 1000 rpm. Symbols are experiments, curves indicate trends.

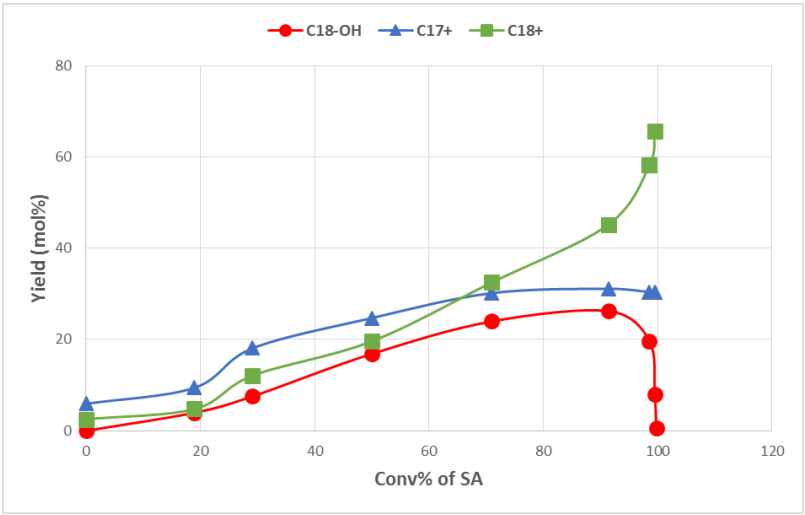

Fig 20: Baseline experiment- HDO of stearic acid (SA) at 300°C, hydrogen pressure 50 bar, catalyst mass 0.4 g, and stirring rate 1000 rpm. Symbols are experiments, curves indicate trends.

4.2.2 Kinetic modeling results

A kinetic model is developed to explain the reaction pathways for HDO of SA. The model was developed based on the results from experimental Section 4.2.1 above, and open literature [16,

20, 24, 40]. A simplified reaction scheme is proposed for HDO of SA for the kinetic model, see Scheme 1. The five main reactions occurring on the NiMoS catalyst surface are – Reaction 1: Conversion of SA to C18=O by reduction of carboxyl group; Reaction 2: Decarboxylation of SA to C17+ hydrocarbon via removal of CO2; Reaction 3: Reduction of C18=O to C18-OH; Reaction 4: Decarbonylation of C18=O to C17+; and Reaction 5: Removal of water from C18-OH to yield C18+ hydrocarbons. It should be noted that octadecanal, rather than the alcohol is considered as the main intermediate. It was observed in Section 4.2.1 that C18-OH is the intermediate when starting from C18=O feed and very little C18=O formed from C18-OH feed. Also, the saturation of double bonds in alkenes (both C17 and C18) have been lumped together since these hydrogenation reactions are quick and straight forward. Carbon oxides would be released from the decarbonation reaction. Additionally, side reactions like water gas shift (WGS) and methanation would contribute to the distribution of CO, CO2 and CH4 in the gas phase. WGS and methanation reactions were initially included in the kinetic model but the predictions from the model for the gas phase were found to be poor. This could be explained due to the fact that the solubility of CO2 in liquid phase is much larger than other two gases as per the liquid-vapor equilibrium predicted by the EOS.

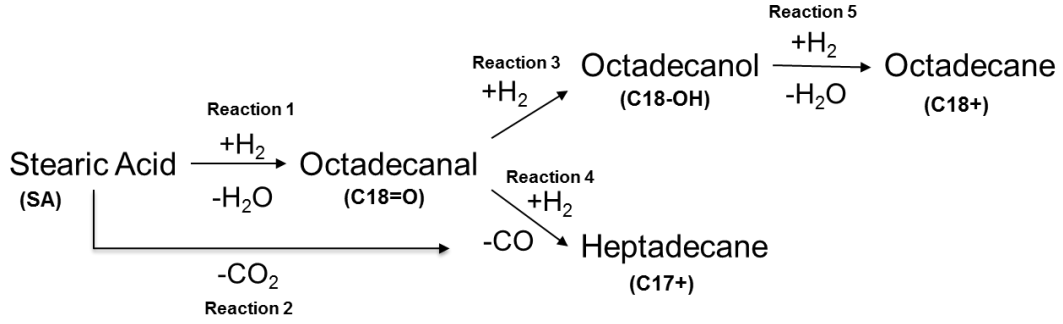

Scheme 1: Simplified reaction scheme for kinetic model

4.2.2.a Kinetic rate expressions

Table 6, presents the Langmuir-Hinshelwood (LH) type rate expressions for the reactions mentioned in Scheme 1. The denominator of the rate expressions include an inhibition term due to SA. This inhibition is in accordance with a few experimental studies in the literature which suggest that species containing a carboxylic group inhibit the HDO reactions [29, 40, 56]. This seems to be validated by our results as discussed in Section 4.2.1 above regarding Fig 20. In the given model it was assumed that there is only one site for all reactions to occur. Thus, the inhibition term for SA was included in all rate expressions. This inhibition term was found to be very important to allow the rate of reaction for C18-OH to increase as less SA remained in the reaction mixture and thus a better agreement between modeling and experimental results could be achieved. The SA inhibition term permitted the effective order of the reaction with respect to SA to be less than unity in Scheme 1 for reactions 1 and 2. This is also in agreement with the results presented in experimental Section 4.2.1 and as shown in Fig 20. Donnis et. al.[20] validated the tautomerism step during HDO of similar molecules. This equilibrium term was included for the direct-HDO route in the rate expressions.

Table 6: Reaction scheme and rate expressions

	Reaction	Rate expression
r1	$C_{18}H_{36}O_2 + H_2 \rightarrow C_{18}H_{36}O + H_2O$	$r_1 = \frac{k_1 C_{SA} C_{H2}}{(1 + K_{SA} C_{SA})}$
r2	Decarboxylation $C_{18}H_{36}O_2 \rightarrow C_{17}H_{36} + CO_2$	$r_2 = \frac{k_2 C_{SA}}{(1 + K_{SA} C_{SA})}$
r3	Direct-HDO $C_{18}H_{36}O + H_2 \rightarrow C_{18}H_{37}OH$	$r_3 = \frac{k_3 C_{C18=O} C_{H2}}{(1 + K_{SA} C_{SA})} \left(1 - \frac{a_{C18OH}}{a_{C18=O} a_{H2} K_{eq}}\right)$
r4	Decarbonylation $C_{18}H_{36}O \rightarrow C_{17}H_{36} + CO$	$r_4 = \frac{k_4 C_{C18=O}}{(1 + K_{SA} C_{SA})}$
r5	$C_{18}H_{37}OH + H_2 \rightarrow C_{18}H_{38} + H_2O$	$r_5 = \frac{k_5 C_{C18OH}}{(1 + K_{SA} C_{SA})}$

4.2.2.b Parameter estimations and simulation results

Table 7, presents the rate and adsorption equilibrium constants for the reactions and their respective activation energies. The reaction rate constants were calculated using all experiments at the baseline temperature of 300 °C, whereas activation energies were calculated based on the deviations at the higher and lower temperatures. The range of the confidence intervals (95%) depicts the accuracy of assessment. In Table 7, it could be seen that the confidence intervals are relatively high for rate constants of reaction 2 and 4 and the activation energy for reaction 4. This could be likely due to the fact that both these reactions led to the formation of products C17+ via decarboxylation and decarbonylation route, and thus their kinetic parameters are correlated. These two routes have been distinguished only at one temperature i.e. 275°C based on the difference in selectivity from the experiments with SA and C18=O as feed. Similarly reactions 1 and 2 are related as both are involved in the conversion of SA. So again correlation likely explains why the confidence interval for the activation energy of reaction 1 is high. A comparison of experimental and modeling results have been shown in Fig 21-24. The continuous lines correspond to the results from the simulations while symbols represent the experimental data. There is a good agreement between the modeling and experimental results in the given range of reaction conditions (temperature 275-325 °C, pressure 40-70 bar hydrogen, feed concentration 2-8 wt%) tested. For instance, the model predicted faster conversion of SA at higher temperature of 325 °C compared to 275 °C as shown in Fig 21. The increase in selectivity for C17+ products with increased temperature was also well-predicted by the model. In Fig 21a and 22, the experiments with varying pressure are depicted. It could be seen that there is a good agreement between the experiment and simulation results with respect to change in selectivity with increase in pressure. The model is able to predict that direct-HDO route is preferred at higher hydrogen pressure. This is in accordance with the reaction scheme where the direct-HDO reaction (reaction 3 in Table 6) is dependent on H2 concentration, whereas the competing decarbonylation (reaction 4) and the decarboxylation (reaction 2) are independent of H2 concentration. Also, the slower rate of conversion of SA with increasing initial feed concentration was consistent with the experimental data in Fig 21a and 23. The inhibition term included in the rate expressions for SA mentioned in the above section facilitates this good agreement. The developed model also predicted the change in concentration profiles when octadecanol and octadecanal feed were employed (see Fig 24). The model closely predicts that direct-HDO is by far the most favored route when C18-OH is used.

This is due to the fact that the C18-OH is an intermediate of only the direct-HDO pathway according to the model reaction scheme (Scheme 1). Similarly, the rapid conversion of C18=O was consistent with the experimental data in Fig 24a which is due to the high reactivity of aldehyde species.

Table 7: Kinetic parameter values and 95% confidence intervals

Rate and adsorption equilibrium constants (units) at 300°C	Value ± Confidence interval	Activation energies (kJ mol^{-1})	Value ± Confidence interval
k_1 (m^6 mol^{-1} kg^{-1} s^{-1})	$5.52\pm1.16\times10^{-5}$	E_1	22.3±17.3
k_2 (m^3 kg^{-1} s^{-1})	$8.63\pm1.96\times10^{-3}$	E_2	119±30.2
k_3 (m^6 mol^{-1} kg^{-1} s^{-1})	$2.78\pm0.53\times10^{-3}$	E_3	159±31.8
k_4 (m^3 kg^{-1} s^{-1})	$4.72\pm2.26\times10^{-2}$	E_4	90.7±80.4
k_5 (m^3 kg^{-1} s^{-1})	$2.70\pm0.34\times10^{-2}$	E_5	117±20.8
K_{SA} (m^3 mol^{-1})	$5.14\pm1.34\times10^{-2}$		

a) 275˚C, 50 bar

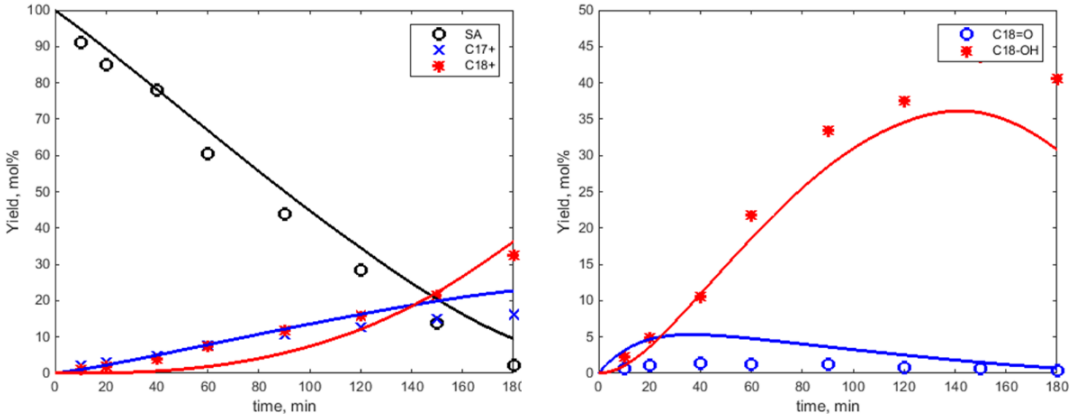

b) 300˚C, 50 bar

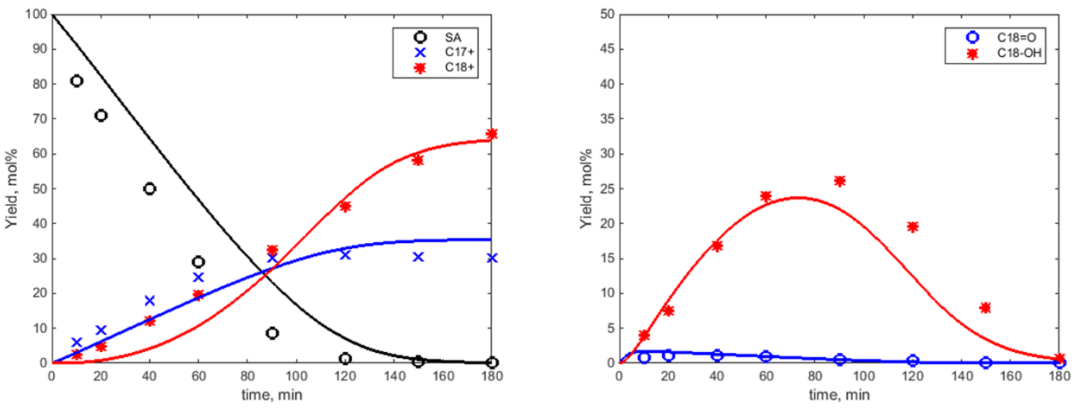

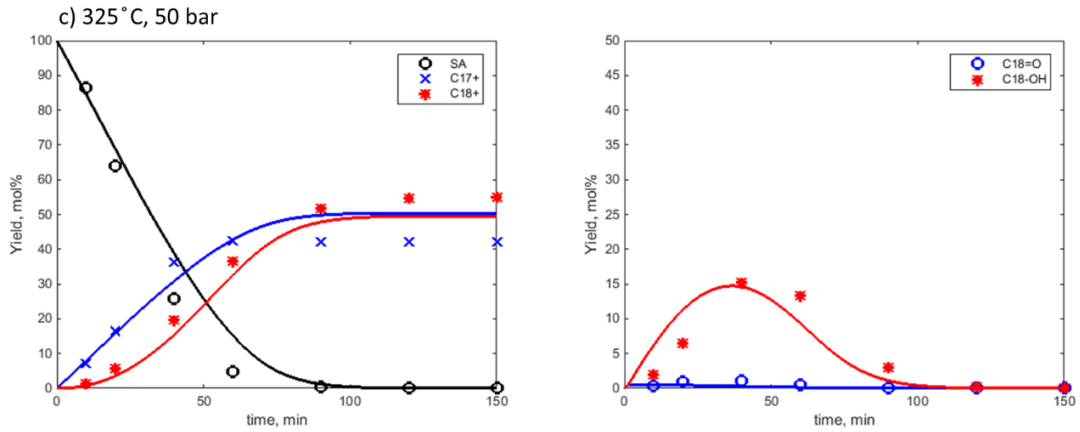

Figure 21: Comparison of experimental and modeled results for varying temperature: (a) 275°C, (b) 300°C, (c) 325°C with hydrogen pressure 50 bar, feed 5 wt% SA, catalyst mass 0.4 g and stirring speed 1000 RPM. Symbols are experiments, curves are model predictions.

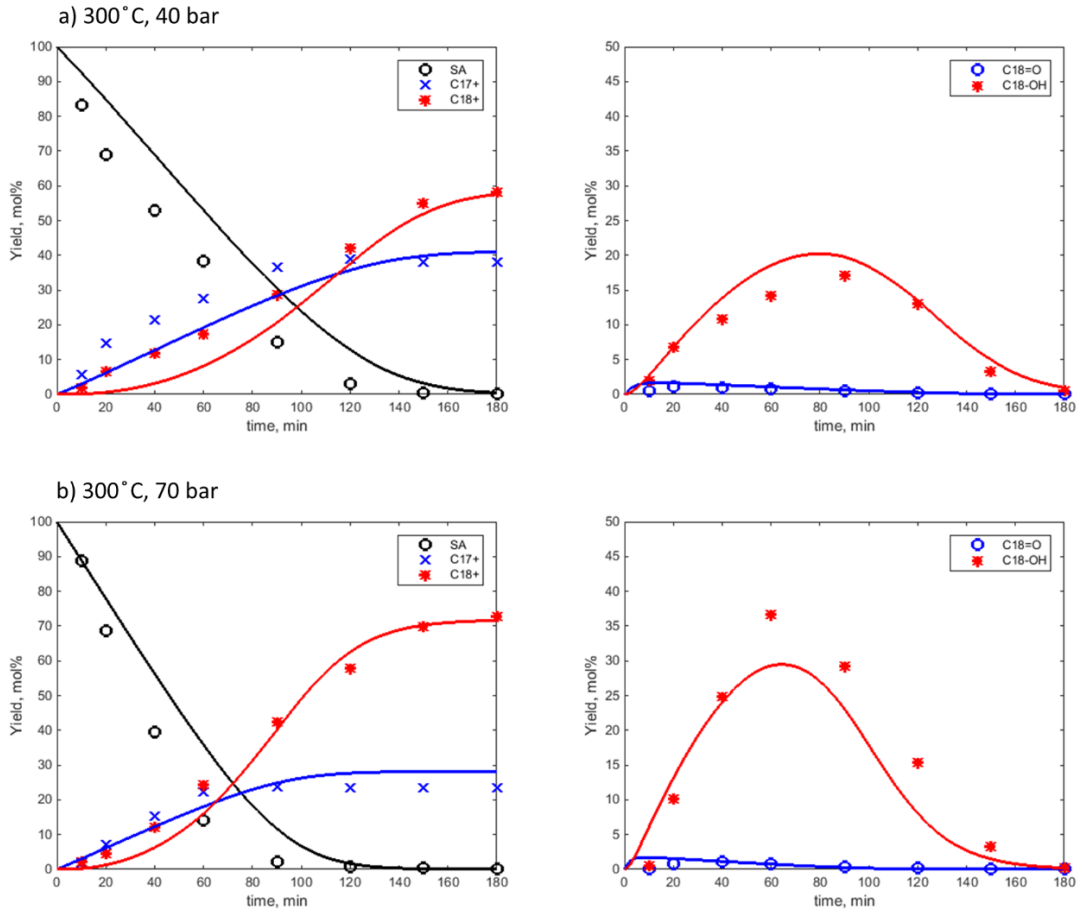

Figure 22: Comparison of experimental and modeled results for varying hydrogen pressure: (a) 40 bar, (b) 70 bar with temperature 300°C, feed 5 wt% SA, catalyst mass 0.4 g and stirring speed 1000 RPM. Symbols are experiments, curves are model predictions.

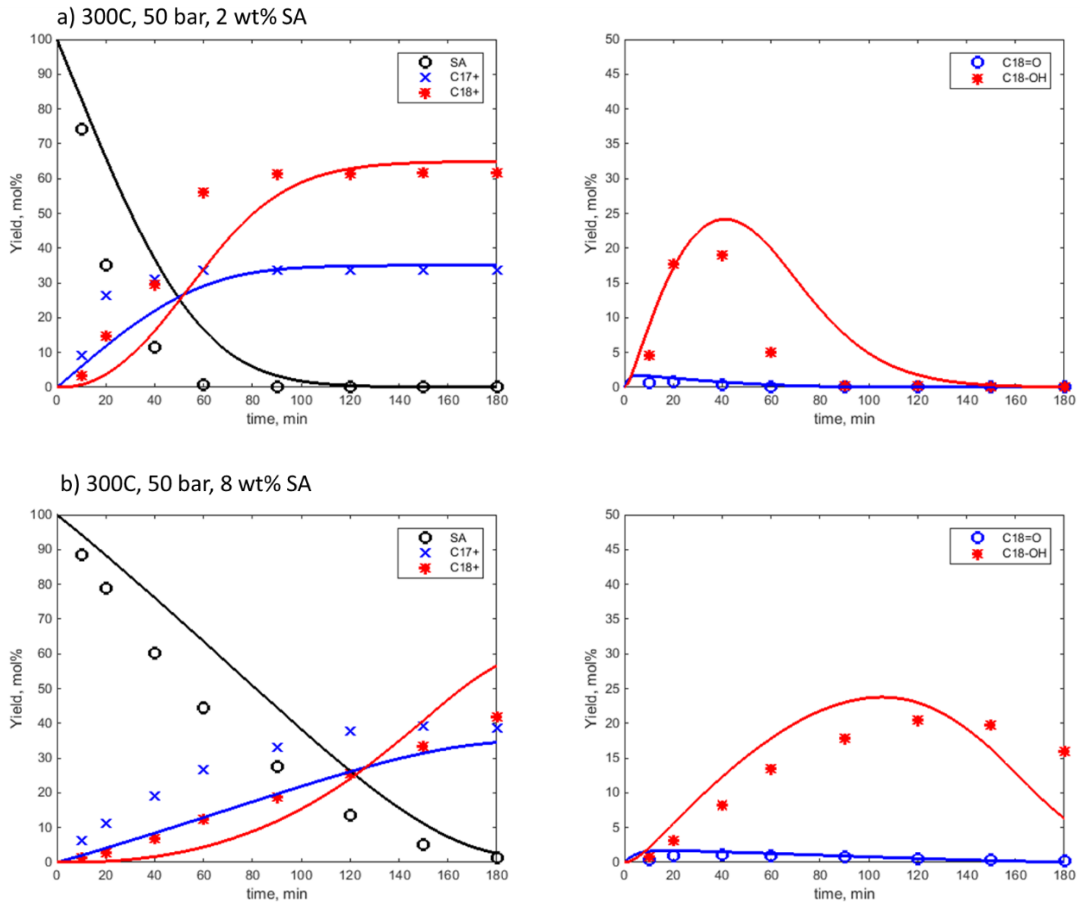

Figure 23: Comparison of experimental and modeled results for varying feed concentration: (a) 2 wt% SA, (b) 8 wt% SA with temperature 300°C, hydrogen pressure 50 bar, catalyst mass 0.4 g and stirring speed 1000 RPM. Symbols are experiments, curves are model predictions.

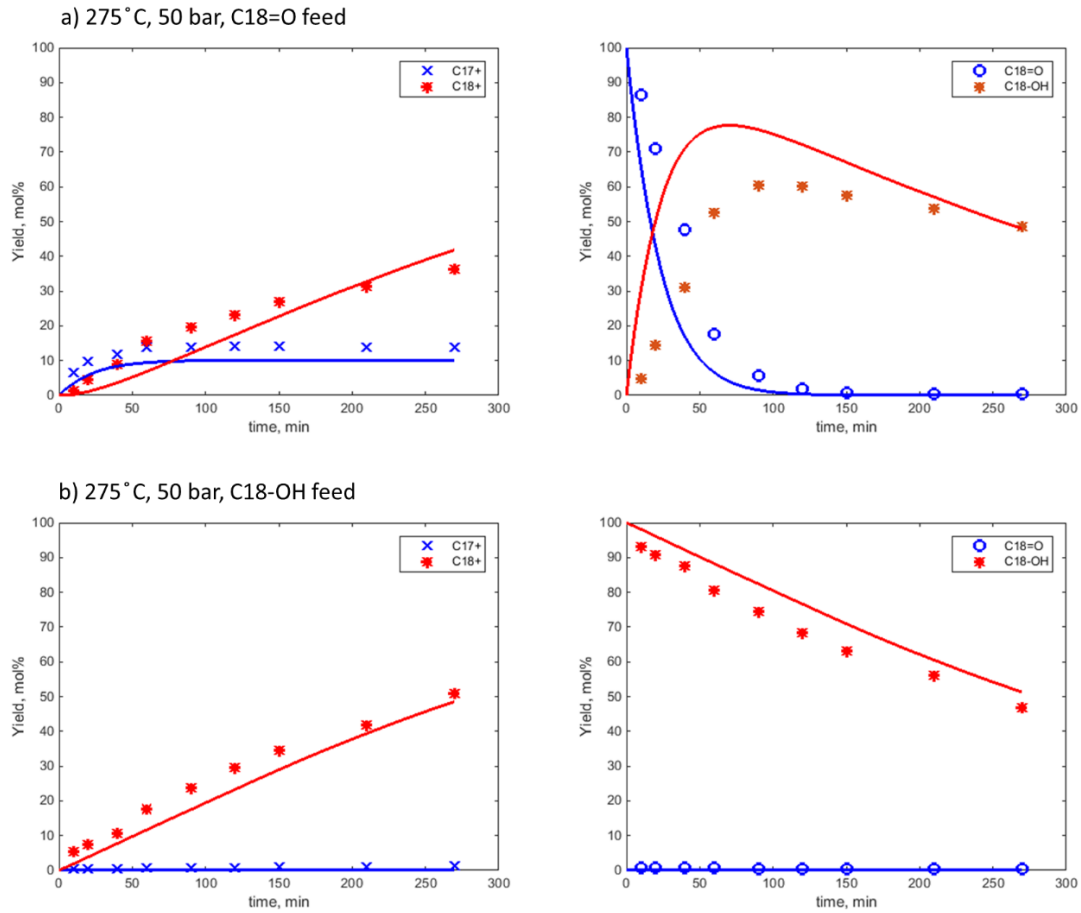

Figure 24: Comparison of experimental and modeled results for varying feed component: a) 5 wt% C18=O, b) 5 wt% C18-OH with temperature 275°C, hydrogen pressure 50 bar, catalyst mass 0.04 g and stirring speed 1000 RPM. Symbols are experiments, curves are model predictions.

5 Conclusions and Outlook

5.1 Concluding Remarks

This thesis includes studies on the deactivation of sulfided NiMo catalysts due to iron species and kinetic modeling of hydrodeoxygenation (HDO) of stearic acid.

The deactivation of molybdenum based catalysts (MoS_2 and NiMoS) supported on alumina was investigated over a range of concentration of Fe during HDO of oleic acid. Renewable feeds are known to have higher total acid numbers (TAN) which could cause corrosion during storage and transportation in iron vessels to give iron salts. Fe oleate complex was used as the poison and added together with the feed and solvent to the batch reactor. This Fe poison had a negative impact on the activity for both unpromoted and promoted catalysts. The conversion of oxygenates slowed down which would not be a desirable scenario in a refining process. Another interesting finding was the change in selectivities for these catalyst systems. C17 hydrocarbons were the major product when NiMoS was employed while for MoS_2 selectivity for C18 hydrocarbons was greater. But, in presence of Fe poison, the selectivity for direct-HDO (C18+) increased for NiMoS while with MoS_2 there was a jump in the selectivity for the decarbonation route (C17+). Spent catalysts were characterized to elucidate reasons behind the observed changes in activity and selectivity. BET results suggest a significant drop in the pore volume which explains the decrease in activity up to a certain extent. This drop in pore volume could not be attributed to the coking since the carbon content of spent catalyst was minimal and independent of the Fe added. A loss of active sulfide phase was also ruled out since the sulfur content of spent catalyst did not show much loss or relation to Fe addition. The results from temperature programmed reaction with hydrogen indicated a loss of labile sulfur instead. This was concluded by the ability to react with hydrogen to produce H_2S for a baseline and a poisoned catalyst sample. TEM-EDX imaging resulted in information of relative distribution of Fe with respect to Ni and Mo. It was found that Fe preferentially deposits around Ni which illustrates the reduced activity and lower selectivity for the C17+ products which otherwise is a preferred reaction route with the NiMoS system. On the other hand, for MoS_2 catalyst, the Fe species would have caused poisoning of active sites and may have formed the less active FeMo phase which explains the drop in activity and switch in the selectivity from direct-HDO to decarbonation.

The reaction scheme for hydrodeoxygenation (HDO) of SA over a NiMo catalyst has been explored in detail by employing Stearic acid (SA), Octadecanal (C18=O) and Octadecanol (C18-OH) as feed components. It was proposed that the aldehyde is the immediate intermediate during the HDO of

SA and not C18-OH based on the experimental results. Several experiments were carried over a range of temperature (275-325 °C), pressure (40-70 bar hydrogen), feed concentration (2-8 wt%) and stirring rate (500-1000 rpm). On the basis of which a simplified reaction scheme for HDO of SA a kinetic model was developed. The estimation for composition of vapor and liquid phases was based on vapor-liquid equilibrium (VLE) calculated from the Predictive Soave-Redlich-Kwong (PSRK) equation of state. An inhibition term due to stearic acid was included in the kinetic rate expressions. The experimentally observed rates of conversions and variations in selectivity for varying temperatures, hydrogen pressure and feed concentrations were well reproduced by the kinetic model. The reaction scheme and contribution of the competing rates of decarboxylation and decarbonylation to produce C17+ products were distinguished by experiments with feed of intermediate species (C18=O and C18-OH).

5.2 Future Work

We observed that a FeMo phase could have formed when Fe poison was employed during hydrodeoxygenation (HDO) of oleic acid over MoS_2 catalyst. It resulted in different activity and selectivity during hydrodeoxygenation of fatty acids in Article I. It has been well established that Ni and Co metals act as the most effective promoters of MoS_2 for hydrodesulphurization (HDS) reactions in particular. For upgrading of renewable feeds from bio-origins, HDO is the key step. There are a few subtle differences in the chemistry of HDO and traditionally studied HDS reactions, including for example selectivity between direct-HDO and decarbonation routes. Therefore, it would be interesting to explore Fe and other transition metals in promotion of molybdenum sulfides specifically for HDO reactions.

In Article II, we developed a kinetic model for hydrodeoxygenation (HDO) of stearic acid (SA) which was employed as a model compound for renewable feed. It would be interesting to validate the kinetic model for a real-world feed like raw tall oil or algal oil to see how well it predicts the experimental results. In the current model, we assumed that the reactions occur only on one site. We could expand on that to explore if different catalytic sites are needed to develop a more mechanistic kinetic model. Experimental studies could be focused on exploring for example whether the carboxylic reactant and hydrogen share, partly share or are on separate sites. This would contribute to the broader understanding of surface reactions during HDO of fatty acids on NiMo catalyst systems.

6 References

[1] BP Energy Outlook 2018, 2018.
[2] B.N.E. Finance, New Energy Outlook 2017, (2017).
[3] EIA, International Energy Outlook 2017, 2017.
[4] S.a.W.C.R.P.t. IRENA, The Power to Change: Solar and Wind Cost Reduction Potential to 2025, June 2016.
[5] E. Mengelkamp, B. Notheisen, C. Beer, D. Dauer, C. Weinhardt, A blockchain-based smart grid: towards sustainable local energy markets, Computer Science - Research and Development, 33 (2018) 207-214.
[6] IEA, World Energy Outlook 2017.
[7] CO2 emissions (metric tons per capita) https://data.worldbank.org.
[8] Swedish Government's climate initiatives.
[9] OPEC, OPEC Annual Statistical Bulletin 2017.
[10] L.G.F. Terry L. Marker, Martin B. Linck, Hydropyrolysis of biomass for producing high quality liquid fuels.
[11] T.A. Milne, R.J. Evans, N. Abatzaglou, Biomass Gasifier"Tars": Their Nature, Formation, and Conversion, National Renewable Energy Laboratory, Golden, CO (US), 1998.
[12] R. Tiwari, B.S. Rana, R. Kumar, D. Verma, R. Kumar, R.K. Joshi, M.O. Garg, A.K. Sinha, Hydrotreating and hydrocracking catalysts for processing of waste soya-oil and refinery-oil mixtures, Catalysis Communications, 12 (2011) 559-562.
[13] H. Aatola, M. Larmi, T. Sarjovaara, S. Mikkonen, Hydrotreated Vegetable Oil (HVO) as a Renewable Diesel Fuel: Trade-off between NOx, Particulate Emission, and Fuel Consumption of a Heavy Duty Engine, SAE International Journal of Engines, 1 (2008) 1251-1262.
[14] Neste Renewable Diesel Handbook.
[15] S.L.a.A.R. B Flach, EU Biofuels Annual 2017.
[16] P. Arora, H. Ojagh, J. Woo, E. Lind Grennfelt, L. Olsson, D. Creaser, Investigating the effect of Fe as a poison for catalytic HDO over sulfided NiMo alumina catalysts, Applied Catalysis B: Environmental, 227 (2018) 240-251.
[17] E. Furimsky, Catalytic hydrodeoxygenation, Applied Catalysis A: General, 199 (2000) 147-190.
[18] P.M. Mortensen, D. Gardini, C.D. Damsgaard, J.-D. Grunwaldt, P.A. Jensen, J.B. Wagner, A.D. Jensen, Deactivation of Ni-MoS2 by bio-oil impurities during hydrodeoxygenation of phenol and octanol, Applied Catalysis A: General, 523 (2016) 159-170.

[19] D. Kubička, J. Horáček, Deactivation of HDS catalysts in deoxygenation of vegetable oils, Applied Catalysis A: General, 394 (2011) 9-17.
[20] B. Donnis, R.G. Egeberg, P. Blom, K.G. Knudsen, Hydroprocessing of Bio-Oils and Oxygenates to Hydrocarbons. Understanding the Reaction Routes, Topics in Catalysis, 52 (2009) 229-240.
[21] S.-J. Lee, S. Go, G.-T. Jeong, S.-K. Kim, Oil production from five marine microalgae for the production of biodiesel, Biotechnology and Bioprocess Engineering, 16 (2011) 561-566.
[22] A. Kumar, S. Sharma, Potential non-edible oil resources as biodiesel feedstock: An Indian perspective, Renewable and Sustainable Energy Reviews, 15 (2011) 1791-1800.
[23] J.M. Anthonykutty, K.M. Van Geem, R. De Bruycker, J. Linnekoski, A. Laitinen, J. Räsänen, A. Harlin, J. Lehtonen, Value Added Hydrocarbons from Distilled Tall Oil via Hydrotreating over a Commercial NiMo Catalyst, Industrial & Engineering Chemistry Research, 52 (2013) 10114-10125.
[24] O.İ. Şenol, E.M. Ryymin, T.R. Viljava, A.O.I. Krause, Reactions of methyl heptanoate hydrodeoxygenation on sulphided catalysts, Journal of Molecular Catalysis A: Chemical, 268 (2007) 1-8.
[25] S. Brillouet, E. Baltag, S. Brunet, F. Richard, Deoxygenation of decanoic acid and its main intermediates over unpromoted and promoted sulfided catalysts, Applied Catalysis B: Environmental, 148–149 (2014) 201-211.
[26] P.M. Mortensen, J.D. Grunwaldt, P.A. Jensen, K.G. Knudsen, A.D. Jensen, A review of catalytic upgrading of bio-oil to engine fuels, Applied Catalysis A: General, 407 (2011) 1-19.
[27] C. Dupont, R. Lemeur, A. Daudin, P. Raybaud, Hydrodeoxygenation pathways catalyzed by MoS2 and NiMoS active phases: A DFT study, Journal of Catalysis, 279 (2011) 276-286.
[28] D.W.S. Wayne K. Craig, Production of hydrocarbons with a relatively high cetane rating, 1988.
[29] E. Laurent, B. Delmon, Study of the hydrodeoxygenation of carbonyl, car□ylic and guaiacyl groups over sulfided CoMo/γ-Al2O3 and NiMo/γ-Al2O3 catalysts: I. Catalytic reaction schemes, Applied Catalysis A: General, 109 (1994) 77-96.
[30] D. Kubička, L. Kaluža, Deoxygenation of vegetable oils over sulfided Ni, Mo and NiMo catalysts, Applied Catalysis A: General, 372 (2010) 199-208.
[31] H. Topsøe, B.S. Clausen, F.E. Massoth, Hydrotreating Catalysis, in: J.R. Anderson, M. Boudart (Eds.) Catalysis: Science and Technology, Springer Berlin Heidelberg, Berlin, Heidelberg, 1996, pp. 1-269.
[32] H. Zhang, H. Lin, Y. Zheng, The role of cobalt and nickel in deoxygenation of vegetable oils, Applied Catalysis B: Environmental, 160–161 (2014) 415-422.
[33] M. Snåre, I. Kubičková, P. Mäki-Arvela, K. Eränen, D.Y. Murzin, Heterogeneous Catalytic Deoxygenation of Stearic Acid for Production of Biodiesel, Industrial & Engineering Chemistry Research, 45 (2006) 5708-5715.
[34] B. Peng, Y. Yao, C. Zhao, J.A. Lercher, Towards Quantitative Conversion of Microalgae Oil to Diesel-Range Alkanes with Bifunctional Catalysts, Angewandte Chemie International Edition, 51 (2012) 2072-2075.
[35] K. Sun, A.R. Wilson, S.T. Thompson, H.H. Lamb, Catalytic Deoxygenation of Octanoic Acid over Supported Palladium: Effects of Particle Size and Alloying with Gold, ACS Catalysis, 5 (2015) 1939-1948.
[36] E. Laurent, B. Delmon, Study of the hydrodeoxygenation of carbonyl, car□ylic and guaiacyl groups over sulfided CoMo/γ-Al2O3 and NiMo/γ-Al2O3 catalyst: II. Influence of water, ammonia and hydrogen sulfide, Applied Catalysis A: General, 109 (1994) 97-115.

[37] O.İ. Şenol, T.R. Viljava, A.O.I. Krause, Effect of sulphiding agents on the hydrodeoxygenation of aliphatic esters on sulphided catalysts, Applied Catalysis A: General, 326 (2007) 236-244.
[38] I. Simakova, B. Rozmysłowicz, O. Simakova, P. Mäki-Arvela, A. Simakov, D.Y. Murzin, Catalytic Deoxygenation of C18 Fatty Acids Over Mesoporous Pd/C Catalyst for Synthesis of Biofuels, Topics in Catalysis, 54 (2011) 460-466.
[39] E.W. Ping, J. Pierson, R. Wallace, J.T. Miller, T.F. Fuller, C.W. Jones, On the nature of the deactivation of supported palladium nanoparticle catalysts in the decarboxylation of fatty acids, Applied Catalysis A: General, 396 (2011) 85-90.
[40] A.E. Coumans, E.J.M. Hensen, A model compound (methyl oleate, oleic acid, triolein) study of triglycerides hydrodeoxygenation over alumina-supported NiMo sulfide, Applied Catalysis B: Environmental, 201 (2017) 290-301.
[41] H. Ojagh, D. Creaser, S. Tamm, P. Arora, S. Nyström, E. Lind Grennfelt, L. Olsson, Effect of Dimethyl Disulfide on Activity of NiMo Based Catalysts Used in Hydrodeoxygenation of Oleic Acid, Industrial & Engineering Chemistry Research, 56 (2017) 5547-5557.
[42] Y.-J. Lee, K.-W. Jun, J.-Y. Park, H.S. Potdar, R.C. Chikate, A simple chemical route for the synthesis of γ-Fe2O3 nano-particles dispersed in organic solvents via an iron–hydroxy oleate precursor, Journal of Industrial and Engineering Chemistry, 14 (2008) 38-44.
[43] C.J. Easton, L. Xia, M.J. Pitt, A. Ferrante, A. Poulos, D.A. Rathjen, Polyunsaturated Nitroalkanes and Nitro-Substituted Fatty Acids, Synthesis, 2001 (2001) 0451-0457.
[44] Y. Shi, J. Chen, J. Chen, R.A. Macleod, M. Malac, Preparation and evaluation of hydrotreating catalysts based on activated carbon derived from oil sand petroleum coke, Applied Catalysis A: General, 441–442 (2012) 99-107.
[45] T. Holderbaum, J. Gmehling, PSRK: A Group Contribution Equation of State Based on UNIFAC, Fluid Phase Equilibria, 70 (1991) 251-265.
[46] E.-M. Turpeinen, E. Sapei, P. Uusi-Kyyny, K.I. Keskinen, O.A.I. Krause, Finding a suitable thermodynamic model and phase equilibria for hydrodeoxygenation reactions of methyl heptanoate, Fuel, 90 (2011) 3315-3322.
[47] S. Horstmann, A. Jabłoniec, J. Krafczyk, K. Fischer, J. Gmehling, PSRK group contribution equation of state: comprehensive revision and extension IV, including critical constants and α-function parameters for 1000 components, Fluid Phase Equilibria, 227 (2005) 157-164.
[48] J.M.P. B. E. Poling, J. P. O'Connell, Properties of Gases and Liquids, 2001 ed., McGraw-Hill2001.